ACS APPLIED BIO MATERIALS

www.acsabm.org Article

PLGA Nanoplatform for the Hypoxic Tumor Delivery: Folate Targeting, Therapy, and Ultrasound/Photoacoustic Imaging

Abhishesh Kumar Mehata,[⊥] Jyoti Bonlawar,[⊥] Rupen Tamang, Ankit Kumar Malik, Aseem Setia, Shailendra Kumar, Ranadheer Reddy Challa, Bhaskar Vallamkonda, Biplob Koch,* and Madaswamy S. Muthu*

Cite This: https://doi.org/10.1021/acsabm.4c00853 Read Online

ACCESS | Metrics & More | Article Recommendations | Supporting Information

ABSTRACT: Effective targeting of breast tumors is critical for improving therapeutic outcomes in breast cancer treatment. Additionally, hypoxic breast cancers are difficult to treat due to resistance toward chemotherapeutics, poor vascularity, and enhanced angiogenesis, which complicate effective drug delivery and therapeutic response. Addressing this formidable challenge requires designing a drug delivery system capable of targeted delivery of the anticancer agent, inhibition of efflux pump, and suppression of the tumor angiogenesis. Here, we have introduced Palbociclib (PCB)-loaded PLGA nanoparticles (NPs) consisting of chitosan-folate (CS-FOL) for folate receptor-targeted breast cancer therapy. The developed NPs were below 219 nm with a smooth, spherical surface shape. The entrapment efficiencies of NPs were achieved up to 85.78 ± 1.8%. Targeted NPs demonstrated faster drug release at pH 5.5, which potentiated the therapeutic efficacy of NPs due to the acidic microenvironment of breast cancer. In vitro cellular uptake study in MCF-7 cells confirmed the receptor-mediated endocytosis of targeted NPs. In vivo ultrasound and photoacoustic imaging studies on rats with hypoxic breast cancer showed that targeted NPs significantly reduced tumor growth and hypoxic tumor volume, and suppressed angiogenesis.

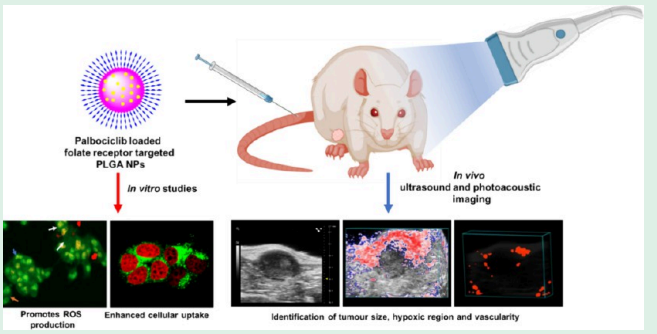

KEYWORDS: *PLGA nanoparticles, breast cancer, folate targeting, Palbociclib, Vit. E TPGS*

1. INTRODUCTION

The most common kind of malignancy among women is breast cancer, which results from estrogen/progesterone receptor mutations.[1] Most people who have this disease are women who are at least 50 years old. Men have a very low probability of developing breast cancer, while it does occur frequently in women.[2] Globally, mammary cancer in women has already overtaken pulmonary cancer as the leading cause of cancer incidence in 2020, with 2.3 million new cases or 11.7% of cancer cases and 6.9% of cancer deaths.[3] Breast cancer is categorized into numerous groups based on several factors, such as the origin, treatment response, molecular characteristics, and clinical presentation. Breast cancer may be estrogen receptor-positive, progesterone receptor-positive, or human epidermal growth factor receptor 2-positive breast cancer.[4,5] The treatment of breast cancer involves partial mastectomy or complete mastectomy, followed by radiotherapy. However, the complete mastectomy may prolong the survival of patients.[6] Chemotherapy may be used after mastectomy to eliminate the breast cancer cells completely.[7] Although chemotherapy extends the survival of cancer patients, there are various drawbacks to delivering it to the patient. The drawbacks associated with traditional anticancer agents include the inability to distinguish between tumor and healthy tissue and drug resistance. Nanotechnology is widely employed to overcome these drawbacks, and it also reduces dosage quantity as well as adverse effects.[8]

Moreover, nanocarriers selectively deliver the drug within targeted tissues.[9,10] Several properties of polymeric NPs make them suitable for sustained and controlled drug delivery systems, including drug protection, biocompatibility, and biodegradability.[11,12] Polymeric NPs are easy to synthesize, purify, and functionalize, and they possess target-specific drug delivery characteristics.[13,14] Palbociclib (PCB) is used to treat metastatic or advanced HR-positive or HER2-negative mammary tumors in combination with other anticancer drugs.[15] Palbociclib selectively inhibits the cyclin-dependent kinase CDK4/6. The growth and division of cancer cells are

Received: June 25, 2024
Revised: July 23, 2024
Accepted: July 26, 2024

stimulated by CDK4 and CDK6 proteins.[16] Poly(lactic-*co*-glycolic acid) (PLGA) is a US-FDA-approved polymeric material[17] that is widely employed in drug delivery systems due to biocompatibility, minimal toxicity, sustained and controlled release behavior.[18,19] PLGA is a biodegradable polymeric material hydrolyzed into its monomeric form (lactic acid and glycolic acid) by esterases. Each monomeric unit is metabolized into the body by regular metabolic pathways such as lactic acid entering into the tricarboxylic acid cycle and glycolic acid converted to glycine.[20] Chitosan is a polycationic biopolymer with broad biomedical applications due to its distinctive chemical behavior, positive charge, and presence of reactive hydroxyl and amino groups.[21] Chitosan is biodegradable, biocompatible, and bioadhesive in nature, degraded by lysozymes, with further metabolism, it will be excreted from the body.[22,23] D-α-tocopheryl polyethylene glycol 1000 succinate (Vitamin E TPGS or TPGS) is a new nonionic surfactant with amphipathic capabilities.[24,25] Its abilities to emulsify, disperse, gel, and solubilize poorly water-soluble medicines have been the subject of extensive research.[26] TPGS has been used to combat multidrug resistance and enhance the oral bioavailability of various anticancer medications.[27] TPGS is the FDA-recognized safe pharmaceutical excipient, and numerous TPGS-based drug delivery systems have been reported.[28] TPGS easily break down into Vitamin E and PEG, which are further metabolized in the liver by CYP4F2, and are excreted in bile and urine.[29] 7,12-Dimethylbenz[a]-anthracene (DMBA) is a potent carcinogen, and when administered subcutaneously to the breast pad of the female rat, it produces a breast tumor of stable size within two months. DMBA-induced breast tumor poses similar characteristics to those of MCF-7 cells.[30] Studies have reported that DMBA-induced breast tumors are hypoxic in nature and pose difficulties in treatment with conventional therapy.[31] Additionally, previous studies reported that breast cancer is overexpressed with the Folate receptor (FRα), and 30−40% of breast cancer cells had FRα overexpression. The overexpression of the FRα related to the higher metabolic demand of folic acid (FOL) for DNA synthesis and repair.[32]

FOL gets metabolized by dihydrofolate reductase and then tetrahydofolate.[33] Hence, designing a drug delivery system having FRα targeting ligand can significantly boost the receptor-based cellular internalization of the loaded drug content. Furthermore, real-time monitoring of the distribution of nanoformulation at targeted tumor sites requires loading of nanoformulation with an imaging/contract agent. Methylene blue (MB) is a versatile dye that has been explored for various imaging studies due to its biocompatibility nature and strong absorption in the near-infrared (NIR) region. Hence, nanoformulation loaded with MB serves as a tool for tracking the homing of the delivery system within the tumor. Ultrasound and photoacoustic imaging system is the preferred noninvasive imaging system for locating the distribution of the MB or MB-loaded nanoformulation at the tumor site.[34,35] Recently, Rajana et al., developed FOL-functionalized lipopolymeric nanoparticles for the delivery of PCB to breast cancer cell lines. This study explored the in vitro efficacy of the developed formulation. However, the formulation does not have diagnostic properties and was not evaluated for in vivo efficacy.[36] In another study, Dhamija et al. developed PCB-loaded redox-sensitive NPs as a smart drug delivery for breast cancer treatments. However, this study explored the therapeutic efficacy in vitro and in vivo models, but the designed delivery system was not for active targeting of overexpressed folate receptors in breast cancer.[37]

In this research article, we aimed to study the targeting effects of the PCB-loaded, folate receptor-targeted PLGA NPs in close comparison with those of nontargeted NPs. It was hypothesized that the incorporation of a chitosan-folate (CS-FOL) conjugate to PLGA NPs enhances the therapeutic efficacy and targeting capability of PCB in breast cancer therapy. Specifically, the chitosan component of the CS-FOL coating plays a crucial role in improving NPs stability, cellular uptake, and controlled drug release, while also providing a nonhemolytic and biocompatible delivery system. First, we synthesized nontargeted and targeted nanoformulation by a single emulsification-solvent evaporation technique. Different physicochemical properties of prepared NPs were characterized, such as zeta potential, particle size, polydispersity index (PDI), scanning electron microscopy (SEM), Transmission Electron Microscopy (TEM), etc. All of the results established that the prepared NPs are of appropriate size and shape. Furthermore, we performed X-ray photoelectron spectroscopy (XPS), X-ray diffraction (XRD), and Fourier transform infrared spectroscopy (FTIR) studies. Safety assessment of prepared NPs with blood and a hemolytic assay was also performed. Prepared NPs were nonhemolytic to human blood, and they proved to be safe. After that, cellular uptake, in vitro cytotoxicity, apoptosis, and histopathology studies were also conducted. In addition, DMBA-induced breast cancer rats were used to assess the in vivo targeting efficiency and anticancer effectiveness of the NPs by using ultrasound/photoacoustic techniques.

2. MATERIALS AND METHODS

2.1. Materials. From Sun Pharma, a gift sample of palbociclib (PCB) was obtained. PLGA (50:50) was obtained from Sigma Aldrich. 1-Ethyl-3-(3-(dimethylamino)propyl) carbodiimide hydrochloride (EDC) and high molecular weight chitosan (MW 30 k Da, based on viscosity, degree of deacetylation ≥90%) were procured from Sisco Research Laboratory Pvt. Ltd., Antares Health Products, Inc. offered D-alpha-tocopheryl-polyethylene glycol-1000-succinate (TPGS) was obtained as a gift sample. The folic acid (FA) supplier was Loba Chemie, Pvt. Ltd. in Mumbai, India. Spectrum Laboratories Inc. provided a 1KDa molecular weight dialysis membrane (Spectra/Por7). Ethanol and dimethyl sulfoxide were purchased from Merck in Darmstadt, Germany. The MCF-7 cell line was procured from NCCS Pune, India. Cell clone (Geneticx Biotech Asia Pvt. Ltd) provided 12-well cell culture plate, 6-well culture plate, T-25 cell culture flasks. DMEM, FBS, Trypsin-EDTA, and Penicillin-Streptomycin (antibiotic) solution were purchased from Gibco. Additionally, 96 cell plates and T-25 cell culture flasks were procured from Eppendorf. In addition, only pure analytical-grade chemicals and reagents were used.

2.2. Methods. *2.2.1. Synthesis of Chitosan-folate (CS-FOL) Conjugate.* Cross-linked CS-FOL was prepared by employing carbodiimide cross-linking with minor changes to already described processes.[38] An EDC (76 mg) and FA (44 mg) were solubilized in anhydrous DMSO (15 mL) and agitated at room temperature for 1 h. CS (153 mg) was dissolved in pH 4.7 acetate buffer to prepare a 0.6% (w/v) chitosan solution. Chitosan solution was transferred to the FA solution and agitated for 16 h in the dark. After that, aqueous NaOH was incorporated dropwise into the solution mentioned above, until the pH reached 9.0. The resulting preparation was centrifuged at 6000 rpm for 5 min. The supernatant was discarded, the formed pellets were collected and washed with distilled water twice, and the resultant brownish precipitate formed was stored in the refrigerator.[39]

2.2.2. CS-FOL Characterization. Fourier-transform infrared spectroscopy (FTIR) technique was employed to analyze the synthesized CS-FOL conjugate.

https://doi.org/10.1021/acsabm.4c00853
ACS Appl. Bio Mater. XXXX, XXX, XXX−XXX

Table 1. Formulation of Different PLGA-Based Nanoparticles[a]

batches	PLGA (mg)	CS (mg)	TPGS (mg)	PCB (mg)	CS-FOL (mg)	MB (mg)	CM6 (mg)
PLGA-CS-NPs	20	8.75	5				
PCB-PLGA-CS-NPs	20	8.75	5	3			
PCB-PLGA-CS-FOL-NPs	20	3.75	5	3	5		
MB-PLGA-CS-NPs	20	8.75	5			0.3	
MB-PLGA-CS-FOL-NPs	20	3.75	5		5	0.3	
CM6-PLGA-CS-NPs	20	8.75	5				0.3
CM6-PLGA-CS-FOL-NPs	20	3.75	5		5		0.3

[a]PLGA: Poly lactic-*co*-glycolic acid. TPGS: D-α-Tocopheryl polyethylene glycol 1000 succinate. PCB: Palbociclib. CS: Chitosan. MB: Methylene Blue. CM6: Coumarin 6. PLGA-CS-NPS: Blank NPs. PCB-PLGA-CS-NPs: PCB-loaded non-targeted NPs. PCB-PLGA-CS-FOL NPs: PCB-loaded folate-targeted NPs. MB-PLGA-CS-NPs: Methylene blue-loaded non-targeted NPs. MB-PLGA-CS-FOL-NPs: Methylene blue-loaded targeted NPs. CM6-PLGA-CS-NPs: Coumarin 6 loaded non-targeted NPs. CM6-PLGA-CS-FOL-NPs: Coumarin 6 loaded targeted NPs.

2.2.3. Degree of Folate Conjugation. A multimode microplate reader was used to assess the amount of FOL conjugation to CS. In brief, CS-FOL conjugate (2 mg) was stirred for 6 h in a 10 mL combination of dichloromethane and dimethyl sulfoxide (1:4). UV spectroscopy was used to analyze the supernatant of the centrifuged samples. The FOL calibration curve was employed to determine the content of folate at a wavelength of 282 nm wavelength. The following formula was used to calculate the amount of FOL conjugation.[40]

$$\text{Amount of FOL conjugation} = \frac{\frac{c}{M}}{(\text{csf} - f)/m}$$

where c is the FOL concentration measured by UV spectroscopy, M is the folic acid's molar mass, csf is the total amount of CS-FOL consumed, and m is the molar mass of one unit of CS.[41]

2.2.4. Synthesis of Nontargeted NPs (PCB-PLGA-CS-NPs) and Targeted NPs (PCB-PLGA-CS-FOL-NPs). The emulsification and solvent evaporation technique was used to prepare nontargeted PCB-loaded PLGA NPs (PCB-PLGA-CS-NPs) and folate receptor targeted NPs (PCB-PLGA-CS-FOL-NPs). Briefly, the organic phase was made by dissolving 20 mg of PLGA and 3 mg of PCB in 2 mL of DCM. The 2.5 mL of glacial acetic acid has been further diluted to 7.5 mL, containing 5 mg of TPGS and 8.75 mg of CS. The aqueous phase was mixed with the organic phase, and then the resultant mixture was ultrasonicated for 4 min using a probe-sonicator. To evaporate the solvent, the produced emulsion was stirred for 2 h using a magnetic stirrer at 710 rpm. A similar method was used to prepare targeted NPs. In this preparation, 5 mg of chitosan folate and 3.75 mg of chitosan were transferred to the aqueous phase instead of 8.75 mg of chitosan. The rest of the process was the same.[42] Similarly, the MB-loaded PLGA NPs were prepared, as mentioned above. First, the aqueous phase was prepared, and then, in the organic phase, instead of 3 mg of PCB, 1 mL of methylene blue of 0.3 mg/mL concentration was added, after which the mixture was subjected to 4 min of ultrasonication using a probe-sonicator. The solvent was evaporated from the resulting emulsion by stirring it with a magnetic stirrer set at 710 rpm for 2 h.

Furthermore, CM6-PLGA-CS-NPs and CM6-PLGA-CS-FOL-NPs were synthesized by employing the same procedure mentioned above. Here, 0.3 mg of coumarin 6 (CM6) solution was transferred to the organic phase instead of 3 mg of PCB followed by exposing the resulting mixture to 4 min of ultrasonication using a probe-sonicator. A magnetic stirrer was used to agitate the resulting emulsion for 2 h to evaporate the solvent. The detailed formulation composition has been presented in Table 1.

The formulation containing PCB (drug) will be used for investigating the treatment effect of the developed formulation, whereas CM6- (fluorescent dye) and MB (NIR sensitive dye)-loaded formulations were used for accessing in vitro cellular uptake and in vivo tumor distribution, respectively.

2.3. Characterization of Nanoparticles. *2.3.1. Zeta Potential and Size Distribution of Nanoparticles.* Zeta potential (ZP) and size distribution of nontargeted and targeted NPs were measured using a Zeta-sizer Nano ZS (DLS, Nano ZS90, Malvern Panalytical, UK) with a 4.0 mV He−Ne laser (633 nm). Measurements were made in triplicate using a solution's refractive index of 1.49 and an absorption of 0.010 at 25 ± 0.1 °C. Run durations and run counts were automatically determined. Electrophoretic light scattering (ELS) technology with Nano ZS (Malvern, Worcestershire, UK) was used to calculate the surface charge and zeta potential value of nanoparticles. The experiment was conducted at 25 ± 0.1 °C in a folded capillary cell. Measurements were taken in triplicate at an absorption of 0.010 and a refractive index of 1.49. The voltage selections and measurement durations were both set to automatic. After diluting (five times) the samples with ultrapure water, all measurements were taken at a 90° scattering angle.[43]

2.3.2. Field Emission Scanning Electron Microscopy. PCB-PLGA-CS-NPs and PCB-PLGA-CS-FOL-NPs surface morphologies were examined using FEI (SEA.) Pvt. Ltd. USA company's Nova Nano SEM 450 instrument. SEM images were acquired at 15 kV voltage and 100−250 KX magnification. Each sample was diluted five times with milli-Q water before being placed on a microscope slide and then dried at 40 °C for the entire night in a forced-air circulating oven. The carbon-coated slides were subjected to SEM imaging.[44]

2.3.3. Transmission Electron Microscopy (TEM). TEM instrument of Tecnai G2 20 TWIM was employed to assess the structural characteristics of PCB-PLGA-CS-NPs and PCB-PLGA-CS-FOL-NPs. Prepared NP formulations were sonicated for 2 min after five dilutions with Millipore water. Afterward, a single drop of diluted sample was applied on carbon-coated TEM grids, dried for 24 h. under vacuum, and then observed under TEM.[45]

2.3.4. Surface Chemistry (XPS). The atomic composition of PCB-PLGA-CS-NPs and PCB-PLGA-CS-FOL-NPs was studied using X-ray photoelectron spectroscopy (XPS). XPS was performed using K-Alpha, Thermo Fisher Scientific USA. The binding energy between 100 and 800 eV was used to identify the elements on the surface of NPs. A drop of concentrated NP suspension was cast on a microscope slide and dried overnight under a vacuum. Finally, XPS analysis of the prepared samples was performed.[46]

2.3.5. Degree of Folate Conjugation in the NPs. A multimode microplate reader was used to measure the amount of folate present in the PCB-PLGA-CS-NPs and PCB-PLGA-CS-FOL-NPs. Briefly, 200 μL of each nanoformulation were lyophilized and solubilized in a 4:1 mixture of DMSO: DCM. Afterward, samples were centrifuged after being vortexed for 6 h. Furthermore, UV−visible spectroscopy was employed to examine the filtered supernatant. The total amount of FOL in the PCB-PLGA-CS-FOL-NPs was calculated by using the calibration curve of FOL at λ_{max} of 282 nm. FOL amount in percentage was calculated using the provided formula,[41]

$$\text{Degree of folate conjugation} = \frac{\text{Amount of folate measured within NPs}}{\text{Total folate content used in NPs}} \times 100$$

2.3.6. X-ray Diffraction Studies. Drug and excipient crystallinity and other physical changes after being converted into formulation were assessed by using XRD. In addition, this analysis was utilized to

https://doi.org/10.1021/acsabm.4c00853
ACS Appl. Bio Mater. XXXX, XXX, XXX−XXX

detect the integrity of the sample constituent. Rigaku Japan XRD instrument was used to obtain the spectrum of CS, FOL, PCB, TPGS, PCB-PLGA-CS-NPs, and PCB-PLGA-CS-FOL-NPs. The diffractograms were acquired at 2θ values ranging from 5 to 80° by employing Ni-filtered Cu Kα as a radiation source; 40Kv tube voltage was utilized with 10° min/scan speed.[47]

2.3.7. Differential Scanning Calorimetry Studies. The melting and transition temperature compatibility of the excipients (PLGA, CS, FA, CS-FOL, TPGS), physical mixture (PM) of all excipients, and drug (PCB) were determined using a DSC-60 Plus with 50 mL per min nitrogen flow rate. Temperatures between 25−500 and 10 °C per min heating rate were used for this study. The heating procedure was carried out using the typical aluminum pan. An empty and loosely covered aluminum pan was used as a reference. Finally, thermograms were obtained.[48]

2.3.8. Thermogravimetric Analysis (TGA). TGA-50 M/s Shimadzu instrument was utilized to evaluate the thermal stability of PCB in PCB-PLGA-CS-NPs and PCB-PLGA-CS-FOL-NPs. The heat from 25 to 500 °C was applied to the NPs. The rate of heating was 10 °C/min, while the N_2 flow rate was maintained at roughly 50 mL/min.[49]

2.3.9. Entrapment Efficiency. The efficiency of PCB entrapment into the aforementioned NPs was measured by using a UV spectrophotometer. The 1 mL suspension of NPs was centrifuged at a speed of 10,000 rpm for 1 h. Remi CM-12 Plus centrifuge machine from Mumbai, India, was employed as a cooling centrifuge at 4 °C to protect the formulation from degradation. Afterward, the resulting NPs pellet was redispersed in 1 mL of ethanol and vortexed until uniform dispersion after being rinsed three times with distilled water. It was then sonicated in a water bath for 2 h to break up the NPs. Following that, it was centrifuged for 30 min at 10,000 rpm. Cary 60, Agilent Technologies, USA company UV−visible spectrophotometer was employed to measure the absorbance of the supernatant solution at 365 nm. The entrapment efficiency (EE%) was determined by utilizing the following equation.[50]

$$\mathrm{EE\%}\left(\frac{w}{w}\right) = \frac{\text{Amount of Palbociclib entrapped within nanoparticles}}{\text{Total amount of Palbociclib added to the formulation}} \times 100$$

A similar approach was employed to estimate the EE of nontargeted and targeted PLGA NPs loaded with MB. Concisely, 1 mL suspension of MB-PLGA-CS-NPs and MB-PLGA-CS-FOL-NPs was centrifuged at 14000 rpm for 30 min, and the supernatant was collected. The formulation was protected against degradation using a cooling centrifuge (Remi CM-12 Plus) at 4 °C. The MB concentration in the supernatant, i.e., unentrapped MB, was quantified using a UV−vis spectrophotometer at 585 nm. The percentage of MB loaded in NPs formulation was determined by using the same formula given above.[51] Additionally, a multimode microplate reader was employed to evaluate the entrapment efficiency of CM6 in CM6-PLGA-CS-NPs and CM6-PLGA-CS-FOL-NPs. A rotary evaporator was used to dry 30 μL of CM6-PLGA-CS-NPS and CM6-PLGA-CS-FOL-NPs. The dry material was agitated for 24 h while being combined with 70 μL of methanol. Membrane filtration (0.22 μm) was employed to filter the resultant mixture after being diluted with water for up to 1 mL. Briefly, a 96-well plate was filled with 200 μL of filtered sample, and absorbance was recorded at a wavelength of 462 nm and an emission wavelength of 502 nm in fluorescent mode. The same formula was employed to determine the percent CM6 entrapped in NPs formulations.[52]

2.4. Stability Studies. Targeted and nontargeted formulations were evaluated for the changes in size and PDI after storage at 2−5 and 25 °C for 60 days. Briefly, PCB-PLGA-CS-NPs and PCB-PLGA-CS-FOL-NPs suspensions were stored at room temperature and refrigerator temperature (25, 2−5 °C). Samples were taken at predefined intervals for 60 days, and their physicochemical properties were assessed to evaluate the storage stability of PCB-PLGA-CS-NPS and PCB-PLGA-CS-FOL-NPs.[53]

2.5. In Vitro Studies. *2.5.1. In Vitro Drug Release Study.* The dialysis bag dispersion approach was employed to determine drug release from pure PCB suspension and PCB-PLGA-CS-NPs and PCB-PLGA-CS-FOL-NPs at pH 7.4 and 5.5. A hermetically sealed dialysis bag 1 kDa was filled with the NPs suspension (1 mL) and gently stirred at 200 rpm at 37 ± 0.5 °C. PBS pH 7.4 (50 mL) and acetate buffer pH 5.5 (50 mL) were used as release media to resemble the acidic tumor microenvironment and the blood's pH, respectively. The dialysis medium was replaced with fresh buffer at various intervals. Three-milliliter sampling was carried out at different time intervals, which were 0.08, 0.17, 0.3, 0.5, 1, 2, 4, 8, 12, 24, 48, and 72 h, and an equivalent media volume was replenished to keep the sink in working order. The amount of emitted PCB in the collected samples was measured by using UV−vis spectroscopy. The time point v/s % cumulative drug release graph was plotted.[54]

2.5.2. In Vitro Safety Evaluation. 2.5.2.1. Blood Smear. Concisely, 5 mL of blood was obtained from a healthy person by vein puncturing. Following that, 100 μL of PCB-PLGA-CS-NPs and PCB-PLGA-CS-FOL-NPs, as well as 100 μL of each deionized water, physiological saline (PBS), and 0.3 mg/mL PCB as positive, negative, and drug controls, were incubated with 900 μL of human blood for 24 h at 4 °C. The prepared blood mixes were dropped, and a blood smear was made using conventional preparation methods. The Leishman stain was used to observe the blood cells in air-dried smear samples. The slides were washed with the help of PBS (7.4 pH) to remove excess stains and then dried. Finally, air-dried samples were observed using bright-field microscopy.[55]

2.5.2.2. Hemolytic Assay. The hemolysis assay was carried out with minimal modifications to the previously reported procedure. The hemocompatibility of PCB, PCB-PLGA-CS-NPs, and PCB-PLGA-CS-FOL-NPs in healthy individuals' blood was evaluated using hemolytic analysis. Fresh human blood was collected and centrifuged at 3000 rpm for 15 min. The supernatant was removed, and a sterile isotonic solution was used to wash the settled red blood cells. The RBC-containing pellet was diluted with PBS 7.4 (1:10). Following that, 100 μL of RBC suspension was mixed with 900 μL each of the test samples PCB, PCB-PLGA-CS-NPs, and PCB-PLGA-CS-FOL-NPs; 100 μL of RBC suspension was also mixed with 900 μL of PBS pH 7.4 (−ve control) and Millipore water (+ve control). A UV spectrophotometer was employed to analyze the supernatants of samples at 545 nm, incubated for 120 min at 37 °C, and centrifuged for 20 min at 12,000 rpm. The following equation determined the percentage of hemolysis of PCB, PCB-PLGA-CS-NPs, and PCB-PLGA-CS-FOL-NPs.

$$\%\text{Hemolysis} = (\text{Abs Ts} - \text{Abs Nc})/(\text{Abs Pc} - \text{Abs Nc}) \times 100$$

where Abs Ts indicates test samples absorbance, Abs Nc denotes −ve control absorbance, and Abs Pc indicates +ve control absorbance.[56,57]

2.5.3. Cellular Uptake Analysis. For the cellular uptake study, CM6 loaded formulations were used for the observing amount of nanoformulations that were uptaken by cells; briefly, 1×10^5 MCF-7 cells were seeded on a coverslip inside each well of a six-well plate and incubated overnight. After cells attachment to the coverslip, the cells were further treated with free CM6 and CM6-loaded formulations (CM6-PLGA-CS-NPs and CM6-PLGA-CS-FOL-NPs) for 5 h. The cells were then washed with 1 mL of PBS and fixed with paraformaldehyde. Following that propidium Iodide (PI) was added to cells and incubated for staining for 15 min. In addition, cells were visualized under a confocal microscope (CLSM, Leica, Germany).

2.5.4. Ao/EtBr Assay (Apoptosis Study). Using acridine orange (AO) and ethidium bromide (EtBr) dual staining, it was possible to distinguish between living and dead cells after determining the integrity of the cell membrane. This test can discriminate between healthy, early- and late-apoptotic as well as necrotic, cells. In brief, MCF-7 cells were seeded at a density of 5×10^4 cells per well in a 12-well culture plate and were incubated overnight for cell attachment. IC_{50} concentration of PCB-PLGA-CS-FOL-NPs (1.44 μg/mL) was employed to treat MCF-7 cells then kept incubated for 24 h. Lastly, an inverted fluorescent microscope (EVOS live cell imaging

https://doi.org/10.1021/acsabm.4c00853
ACS Appl. Bio Mater. XXXX, XXX, XXX−XXX

Table 2. Average Particle Size (Z_{avg}), Polydispersity Index (PDI), Zeta Potential (ZP), and Drug Entrapment Efficiency (%EE) of Formulated NPs[a]

batches	Z_{avg} (nm) (mean ± SD*)	PDI (mean ± SD*)	ZP (mV) (mean ± SD*)	EE (%) (mean ± SD*)
PLGA-CS-NPs	212.3 ± 5.3	0.128 ± 0.08	14.21 ± 2.1	
PCB-PLGA-CS-NPs	214.7 ± 3.4	0.138 ± 0.02	15.27 ± 3.6	80.96 ± 1.7
PCB-PLGA-CS-FOL-NPs	218.9 ± 1.8	0.185 ± 0.02	22.8 ± 1.9	85.78 ± 1.8
MB-PLGA-CS-NPs	208.3 ± 1.9	0.156 ± 0.03	16.5 ± 3.2	83.58 ± 1.3
MB-PLGA-CS-FOL-NPs	210.4 ± 5.2	0.160 ± 0.05	23.4 ± 1.6	86.04 ± 1.7
CM6-PLGA-CS-NPs	206.2 ± 7.4	0.154 ± 0.09	19.2 ± 2.3	80.23 ± 1.5
CM6-PLGA-CS-FOL- NPs	209.2 ± 5.3	0.125 ± 0.04	26.43 ± 1.5	82.36 ± 1.6

[a]PLGA: Poly lactic-*co*-glycolic acid. PCB: Palbociclib. CS: Chitosan. MB: Methylene Blue. CM6: Coumarin 6 Dye. PLGA-CS-NPS: Blank NPs. PCB-PLGA-CS-NPs: non-targeted NPs. PCB-PLGA-CS-FOL-NPs: Chitosan-folate targeted NPs. MB-PLGA-CS-NPs: Methylene blue-loaded non-targeted NPs. MB-PLGA-CS-FOL-NPs: Methylene blue-loaded targeted NPs. CM6-PLGA-CS-NPs: Coumarin 6 loaded non-targeted NPs. CM6-PLGA-CS-FOL-NPs: Coumarin 6 loaded targeted NPs.

equipment from Life Technologies) was used to take pictures in the green and red channels after staining the cells with Ao/EtBr.[58]

2.5.5. In Vitro Cytotoxicity Assay. Cytotoxicity analysis of PCB, PCB-PLGA-CS-NPs, and PCB-PLGA-CS-FOL-NPs was assessed by a standard MTT assay on the MCF-7 cell line (breast cancer cell line). MCF-7 cells were seeded into 96-well plates with DMEM at a density of 1×10^4 cells per well and then cultured overnight for cells to get attached to the flask. The media was discarded, and the cells were treated with the different concentrations of PCB, PCB-PLGA-CS-NPs, and PCB-PLGA-CS-FOL-NPs and then incubated for 24 h. Afterward, the media in each well were replaced with 100 μL of MTT solution (0.5 mg/mL of MTT) and then incubated for 2 h at 37 °C. 100 μL of DMSO was added to the well plates to dissolve the formed formazan crystals.[59] The absorbance was then determined at 570 nm by using a microplate reader. The percent cell viability may be determined by:

$$\text{Cell Viability (\%)} = \left(\frac{\text{At}}{\text{Ac}}\right) \times 100$$

where At − treated cell absorbance and Ac − control cells absorbance.

2.5.6. Reactive Oxygen Species Analysis. Reactive oxygen species analysis was performed by utilizing 2′,7′-dichlorodihydrofluorescein diacetate (DCFH-DA) dye, which will be useful for determining the degree of intracellular ROS production. Briefly, MCF-7 cells were seeded in a 12-well plate at a density of 5×10^4 and incubated overnight for the cell's attachment. The cells were treated with PCB, PCB-PLGA-CS-NPs, and PCB-PLGA-CS-FOL-NPs at the IC_{50} concentration of PCB-PLGA-CS-FOL-NPs for 24 h. The cells were then incubated with 10 μM of DCFH-DA for 30 min at 37 °C after washing with PBS. Additionally, to measure the amount of reactive oxygen species, DCFH-DA fluorescence in the incubated samples was determined using fluorescence microscopy.[60]

2.6. In Vivo Evaluation. The Institutional Animal Ethics Committee (IAEC), IIT (BHU) Varanasi, authorized the usage of the rats in this research (IAEC approval number IIT(BHU)/IAEC/2023/087). The IIT (BHU), Varanasi, carried out the in vivo investigations in compliance with the IAEC's guidelines. The National Research Council's stringent rules were adhered to in each in vivo experiment.

2.6.1. Histopathological Examination. The safety of PCB-PLGA-CS-NPs and PCB-PLGA-CS-FOL-NPs was investigated by using a histopathology study on Sprague−Dawley rats. The animals were randomly split into four groups with three rats in each group. The produced NPs were given intravenously through the tail vein. The saline control group received saline and the standard group received PCB (control). However, PCB-PLGA-CS-NPs and PCB-PLGA-CS-FOL-NPs were given to the remaining animal groups 3 and 4 at a dose similar to that of 5.9 mg/kg of PCB control. All groups were treated three times in three-day intervals, and then, rats were slaughtered on the 15th day. All animal essential organs, such as the heart, liver, and kidneys, were removed and preserved in a 10% V/V formalin solution. All the organs were processed inparaffin box , and then the sample was sliced using a microtome at a 5-μm thickness. Furthermore, hematoxylin and eosin dyes were used for the staining of prepared sections. Light microscopy (Dewinter microscope) was used to observe the histopathological alterations, and Capture Pro 4.1 software was used to record the images.[61,62]

2.6.2. In Vivo Anti-Tumor Activity by Ultrasound and Photoacoustic Imaging. Photoacoustic and ultrasound imaging was performed on 3−4-month-old Sprague−Dawley rats to visualize tumor volume and hypoxia level changes. First, a 50 mg/kg body weight dose of DMBA (cancer inducer) was injected into the breast pad of SD rats to produce breast cancer tumors. The photoacoustic and ultrasound imaging was used to confirm the formation of a tumor. SD rats were then divided into 4 groups, each containing 3 animals. All animals were administered a 5.9 mg/kg dose three times at intervals of 3 days. Group 1 received saline control; Group 2 was treated with drug (PCB) control; Group 3 was treated with PCB-PLGA-CS-NPs, and Group 4 was treated with PCB-PLGA-CS-FOL-NPs. After each dose, photoacoustic and ultrasound imaging of these animals was performed to visualize the tumor volume and hypoxia level changes. Concisely, rats were sedated with 1.5% isoflurane, and a colorless aqueous warmed ultrasonic gel (Supragel, LCH, France) was inserted between the transducer and skin without any air bubbles. The Visual Sonics Vevo LAZR X System (FUJIFILM Visual Sonics Inc., Canada) was used to image tumors. The tumor volume and hypoxia level were measured at regular intervals. 3D scans of ultrasound images were digitally captured. Coronal plane tumor margins were manually defined by using Vevo1LAB 1.7.2 software. The volume of each coronal slice was then determined by using the software. The hypoxic volumes were evaluated using photoacoustic imaging in OxyHemo-Mode.[63]

2.6.3. In Vivo Tumor Targeting Efficiency. SD rats weighing 200−250 g were used for this experiment. Breast cancer was induced in these rats with the help of DMBA. Animals were then randomly divided into 3 groups each containing 3 animals (n = 3). Group 1 animals received pure MB, group 2 animals were given MB-PLGA-CS-NPs, and group 3 animals were administered MB-PLGA-CS-FOL-NPs at a 12 μg/kg dose. Concisely, rats were sedated with 1.5% isoflurane, and a colorless aqueous warmed ultrasonic gel (Supragel, LCH, France) was inserted between the transducer and skin without any air bubbles. The Visual Sonics Vevo LAZR X System (FUJIFILM Visual Sonics Inc., Canada) was used to image tumors. Photoacoustic excitation was carried out at an optical wavelength of 664 nm. 3D scans of ultrasound images were digitally captured. Software version Vevo1LAB 1.7.2 was used to process the data. The photoacoustic signal was captured before and after the injection of the MB control. Additionally, rats received an intravenous infusion of MB-loaded NPs spaced 30 min apart. The accumulation of MB-loaded NPs and MB control at the site of the breast tumor 30 min post i.v. injection was monitored by photoacoustic and ultrasound images.[64]

2.7. Statistical Analysis. The mean ± standard deviation of three experimental results was used to express all of the experimental data, and GraphPad Prism and OriginPro software were used to calculate the statistical data. The student's t-test was employed to compare

https://doi.org/10.1021/acsabm.4c00853
ACS Appl. Bio Mater. XXXX, XXX, XXX−XXX

entrapment efficiency, mean particle size, and in Vitro data. A statistical analysis was performed using the one-way ANOVA and Student's *t*-test. ± standard deviation was used to represent all values. When $P > 0.05$, then data are considered to be statistically nonsignificant. When P values were found to be below 0.05, data were significant. Additionally, different level of significance was designated as *, **, and *** with *P* values of 0.01, 0.001, and 0.0001, respectively.

3. RESULTS AND DISCUSSION

3.1. Evaluation of CS-FOL. *3.1.1. FTIR Spectroscopy.* The functional groups of the synthesized CS-FOL were identified

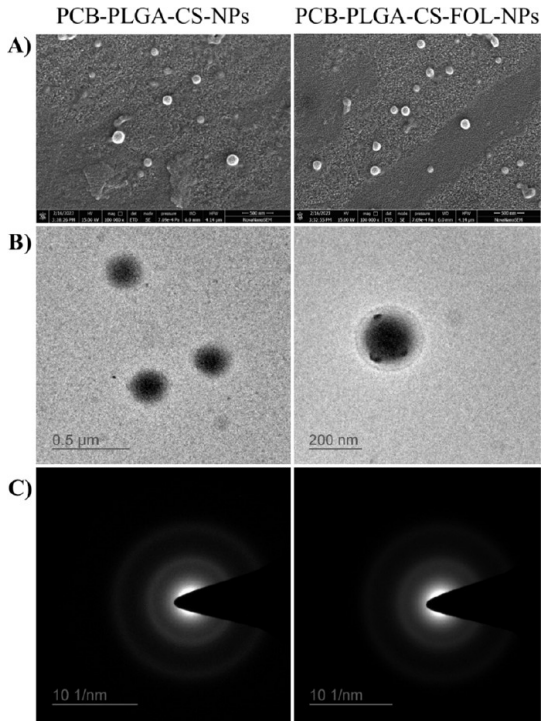

Figure 1. (A) SEM images of nontargeted and targeted nanoformulations. (B) TEM images of nontargeted and targeted nanoformulations. (C) SAED images of nontargeted and targeted nanoformulations.

by investigating the FTIR absorption spectra (Figure S1). The FTIR spectrum of CS exhibits a wide peak in the range of 3662−3107 cm^{-1}, indicating the presence of a hydroxy group that could potentially be combined with NH stretching. In contrast, other characteristic peaks were observed at 2916 cm^{-1} for C−H stretching, 1313 cm^{-1} for C−O stretching, and 1043 cm^{-1} for C−O−C stretching. On the other hand, the FTIR spectrum of FOL displays additional peaks at 1487, 1662, and 838 cm^{-1}, which are associated with C═C aromatic, C═O, and para-disubstituted benzene ring, respectively. However, the peaks related to the C−O and C−O−C stretch were absent. Interestingly, as shown in the figure, the peaks corresponding to the functional groups of CS and FOL are identified in the FTIR spectra of CS-FOL, with minor shifts and variations in the peak intensity.

The FTIR spectra of CS-FOL displayed absorption frequencies of the OH stretch, potentially coupled by an NH stretch band between 3662 and 3072 cm^{-1} with a higher intensity than that of CS (Table S1). The absorption frequencies observed at 1616, 1488, 1337, and 1044 cm^{-1} were identified to be functional groups C═O, C═C, C−O, and C−O−C, respectively. CS-FOL and FOL displayed bending vibrational peaks for primary and secondary amines, whereas CS showed peaks for only primary amines, consistent with their respective chemical structures. Furthermore, the intensity of the peak within the range of 800 to 500 cm^{-1} appears to be higher than that of CS which could be attributed to the combination with the peaks linked to the fingerprint region of FOL, such as those associated with para-disubstituted benzene ring. In conclusion, the chemical structure of CS-FOL was confirmed by detecting its associated spectral features, indicating successful conjugation with FOL.

3.1.2. Amount of FOL Conjugation. UV spectroscopy was used to determine the extent of FOL replacement to chitosan, and the outcomes showed that the extent of FOL modification was approximately 60.37 ± 1.56%.

3.2. Nanoparticle Characterization. *3.2.1. Particle Size, Polydispersity Index, and Zeta Potential of NPs.* The sizes, PDI, and ZP of different PLGA NPs are illustrated in Table 2. The particle size of formulated NPs was in the range of 206.2 ± 7.4−218.9 ± 1.8 nm. The inclusion of CS-FOL on the outermost layer of NPs caused considerable enhancement in the size of particles ($p < 0.05$). The ZP of PCB-PLGA-CS-NPs and PCB-PLGA-CS-FOL-NPs was found to be 15.27 ± 3.6 and 22.8 ± 1.9 mV, respectively. The elevation in the ZP of PCB-PLGA-CS-FOL-NPs was due to the addition of positively charged CS-FOL on the outermost layer of NPs.

3.2.2. Field Emission Scanning Electron Microscopy (FE-SEM). The size and morphology of PCB-PLGA-CS-NPs and PCB-PLGA-CS-FOL-NPs were determined using FE-SEM (FEI Pvt. Ltd., USA). The prepared NPs exhibited a circular shape, were monodispersed, and had a smooth surface, as shown in Figure 1A. All the nanoformulations were near about 200 nm in size and free of cracks and other noticeable defects. Additionally, the DLS analysis of particle size matches the outcomes from FE-SEM.

3.2.3. Transmission Electron Microscopy (TEM). The morphology and shape of developed nanoformulations were evaluated by employing TEM. TEM images of both NPs with nearly 200 nm size are shown in Figure 1B. The obtained data depicted that individual NPs had round morphology with no obvious surface imperfections such as pits and cracks. Images showed monodispersed spherical NPs ranging nearly 200 nm scale. The SAD images for PCB-PLGA-CS-NPs and PCB-PLGA-CS-FOL-NPs revealed diffuse rings, suggesting their amorphous nature.

3.2.4. XPS Analysis. The elemental composition of the developed formulations was investigated using XPS analysis. The obtained XPS data demonstrated the expected peaks for components N, O, and C, as presented in Figure 2A, B. The peaks observed at binding energies of 286−285, 400−399, and 538−532 eV were for C_{1s}, $N_{1s,}$ and O_{1s} respectively. The percentage values of C_{1s}, N_{1s}, and O_{1s} in PCB-PLGA-CS-NPs were 57.99, 2.61, and 39.30%, respectively, whereas, for PCB-PLGA-CS-FOL-NPs, these were 64.4, 2.71, and 32.99%.

3.2.5. Amount of Folate in the NPs. The amount of folate in the PCB-PLGA-CS-FOL-NPs, MB-PLGA-CS-FOL-NPs, and CM6-PLGA-CS-FOL-NPs was evaluated by using UV−visible spectrophotometry, and the FOL content was found to be 64.54, 50.45, and 57.78% respectively.

3.2.6. X-ray Diffraction. The physical state of the NPs was analyzed by employing XRD. Figure 3A shows the XRD overlay spectrum of chitosan, folic acid, chitosan-folate, TPGS,

https://doi.org/10.1021/acsabm.4c00853
ACS Appl. Bio Mater. XXXX, XXX, XXX−XXX

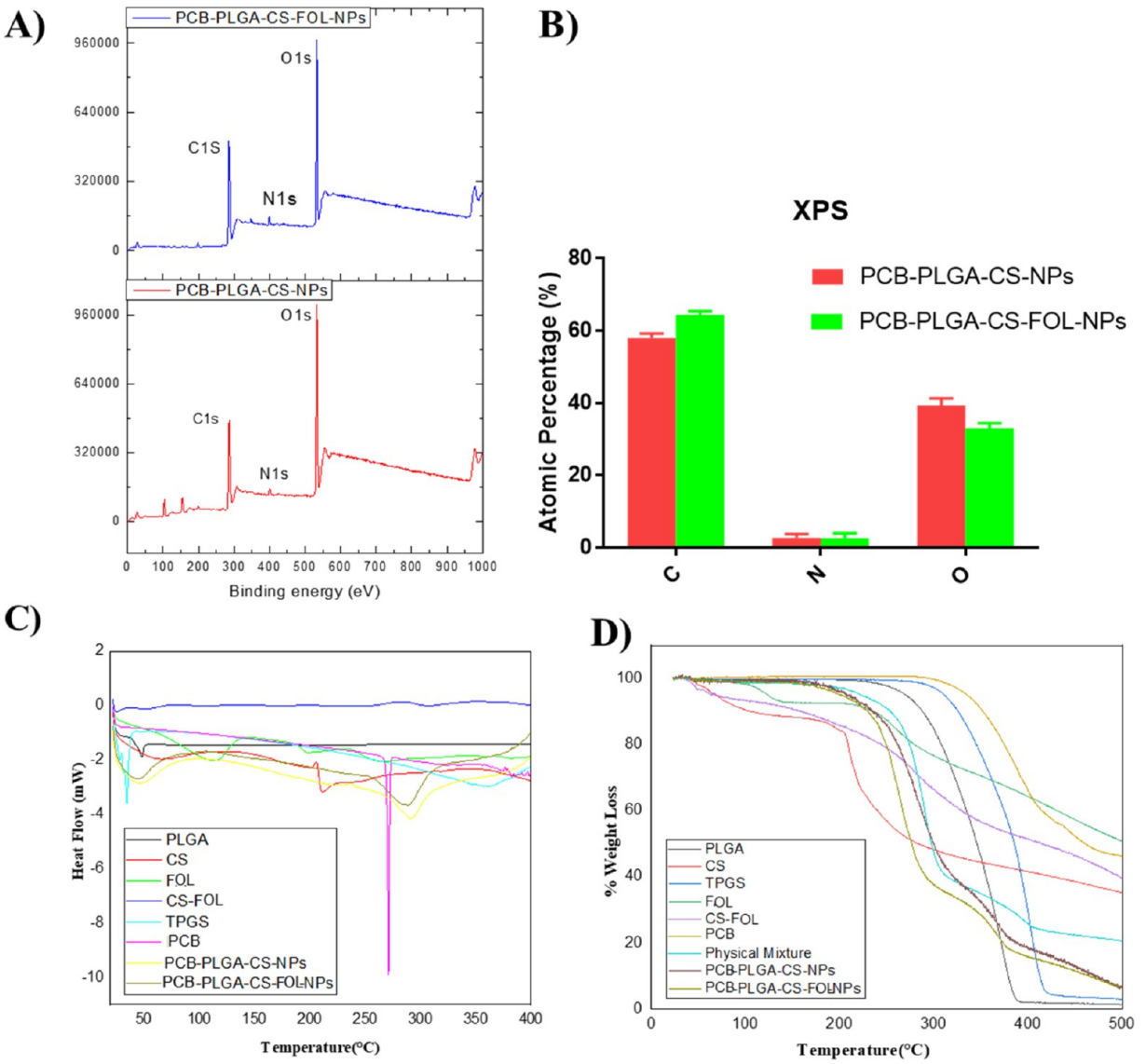

Figure 2. (A) XPS spectra of PCB-PLGA-CS-FOL-NPs and PCB-PLGA-CS-NPs. (B) Elemental composition of PCB-PLGA-CS-NPs and PCB-PLGA-CS-FOL-NPs. (C) DSC thermogram of PLGA, CS, FOL, CS-FOL, TPGS, PCB, PCB-PLGA-CS-NPs, and PCB-PLGA-CS-FOL-NPs. (D) TGA curves of PLGA, CS, TPGS, FOL, CS-FOL, PCB, and Physical Mixture of all excipients, freeze-dried PCB-PLGA-CS-NPs, and PCB-PLGA-CS-FOL-NPs.

PLGA, PCB, optimized PCB-PLGA-CS-NPs, and PCB-PLGA-CS-FOL-NPs. Sharp peaks in the PCB and FA XRD spectra revealed the substance's crystalline form. PCB showed sharp peaks at 2θ values of 7.88°, 10.11°, 11.45°, 17.10°, 19.62°, 22.59°; however, the FOL showed peaks at 2θ values of 10.70°, 13.08°, 16.35°, 26.89°, and 27.78°. The prominent peaks were also detected in the XRD spectrum of chitosan and TPGS, but peaks were less intense, demonstrating their semicrystallinity. The broad peaks were detected in the XRD spectra of PLGA, chitosan, PCB-PLGA-CS-NPs, and PCB-PLGA-CS-FOL-NPs, revealing the amorphous nature of these materials. The peaks observed in the XRD spectra of PCB-PLGA-CS-NPs and PCB-PLGA-CS-FOL-NPs were different from the XRD peaks of PCB, revealing entrapment of the drug within the formulations. A broad peak in the PCB-PLGA-CS-FOL-NPs spectra suggests that the crystalline nature of FOL has been reduced and converted into an amorphous state.

3.2.7. Differential Scanning Calorimtery. The heating characteristics of NPs containing PCB were evaluated by using DSC. Figure 2C depicts the thermograms of PCB, PLGA, TPGS, CS, FOL, PCB-PLGA-CS-NPs, and PCB-PLGA-CS-FOL-NPs. The endothermic peaks of CS, FA, and CS-FOL were detected at 212.16, 114.7, and 281.39 °C, respectively. PCB displayed a sharp endothermic peak at 266.74 °C. However, the endothermic peak of PCB was not detected in PCB-PLGA-CS-NPs and PCB-PLGA-CS-FOL-NPs, indicating successful entrapment of PCB within the nanoformulation.

3.2.8. TGA Analysis. TGA measures a sample's weight variation as a function of temperature. Additionally, the compound stability is discussed. This determines the maximum temperature at which the compound is stable. As illustrated in Figure 2D, CS, FOL, CS-FOL, PLGA, PCB, physical mixture, TPGS, PCB-PLGA-CS-NPs, and PCB-PLGA-CS-FOL-NPs lose 98.06, 98.07, 99.32, 98.09, 99.44, 96.02, 97.06, 98.06, and 97.08% of their initial weight between 25 and 500 °C, respectively. The PCB exhibited an initial reduction in weight at a temperature of 299.93 °C. A gradual

https://doi.org/10.1021/acsabm.4c00853
ACS Appl. Bio Mater. XXXX, XXX, XXX−XXX

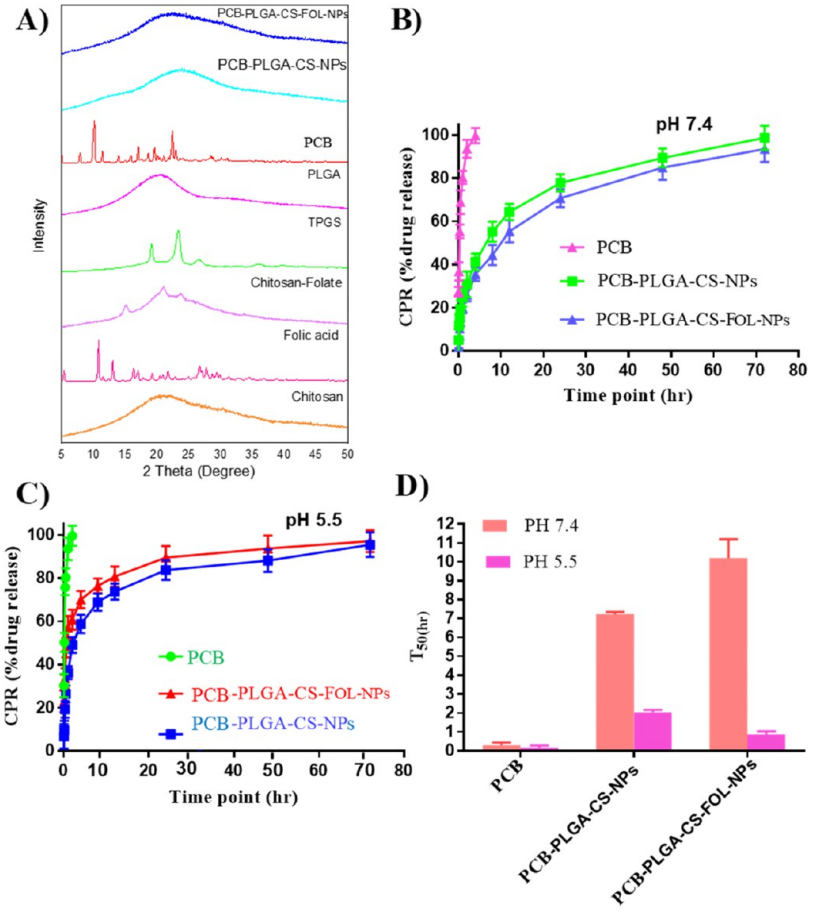

Figure 3. (A) XRD spectra of chitosan, folic acid, CS-FOL, TPGS, PLGA, PCB, PCB-PLGA-CS-NPs, and PCB-PLGA-CS-FOL-NPs. (B) In vitro drug release study of PCB solution, synthesized PCB-PLGA-CS-NPs and PCB- PLGA-CS-FOL-NPs at pH 7.4. (C) In vitro drug release profile of PCB solution, prepared PCB-PLGA-CS-NPs and PCB- PLGA-CS-FOL-NPs at pH 5.5. (D) T_{50} of PCB solution, synthesized PCB-PLGA-CS-NPs and PCB- PLGA-CS-FOL-NPs at pH 7.4 and pH 5.5.

reduction in weight of 42.89% was observed within the temperature range of 300−431.03 °C. Subsequently, a decrease in weight of 9.93% was noted within the range of 432.74−494.52. The PCB-PLGA-CS-NPs exhibit an initial weight reduction of 0.37% at a temperature of 46.16 °C, which can be attributed to water loss. Subsequent to this, a reduction in mass of 59.73% was noted within the temperature range of 171.22−323.30 °C, which was attributed to the degradation of the PLGA, CS, and TPGS polymers. A reduction in weight of 17.31% was observed during the period of 326.49−381.89, which can be attributed to the degradation of PCB. Furthermore, a reduction in weight of 13.85% was noted within the range of 383.49 to 496.01. PCB-PLGA-CS-FOL-NPs result in an initial weight reduction of 0.34% at a temperature of 45.02 °C, which can be attributed to the loss of water. A gradual reduction in weight of 60.45% was noted during the temperature range of 165.18−299.36 °C, which can be attributed to the degradation of PLGA, CS, and TPGS polymers. A reduction in weight of 17.87% was gradually observed within the temperature range of 300.95−378.95 °C, which can be attributed to the degradation of PCB. An additional reduction in weight of 11.54% was noted within the temperature range of 380−495.89 °C. Moreover, 50% weight loss was observed at 279 °C (CS), 344 °C (PLGA), 459.87 °C (PCB), 413.58 °C (CS-FOL), 495.3 °C (FOL), 385.77 °C (TPGS), 296.51 °C (physical mixture), 299.47 °C (PCB-PLGA-CS-NPs) and 275.19 °C (PCB-PLGA-CS-FOL-NPs), indicating the high thermal stability of PCB-PLGA-CS-NPs and PCB-PLGA-CS-FOL-NPs.

3.2.9. Entrapment Efficiency (EE). The EE of PCB-PLGA-CS-NPs and PCB-PLGA-CS-FOL-NPs was found to be 80.96 ± 1.7 and 85.78 ± 1.8%, respectively (Table 2). There was a slight increase in PCB EE in the case of targeted NPs due to the conjugation of CS-FOL on the surfaces of NPs. The EE of MB-loaded targeted (MB-PLGA-CS-FOL-NPs) and non-targeted (MB-PLGA-CS-NPs) NPs were 83.58 ± 1.3 and 86.04 ± 1.7%. In contrast, EE of CM6-loaded nontargeted (CM6-PLGA-CS-NPs) and targeted (CM6-PLGA-CS-FOL-NPs) NPs was found to be 80.23 ± 1.5 and 82.36 ± 1.6%, respectively (Table 2).

3.3. Stability Studies. Long-term stability experiments revealed no discernible variation in PDI or particle sizes when PCB-PLGA-CS-NPs and PCB-PLGA-CS-FOL-NPs were stored at 25 and 2−5 °C. As with the stability data provided in Figure 4C−F, no discernible alteration in particle sizes was found between freshly synthesized and stored NPs, revealing the long-term stability of prepared NPs. Moreover, agglomeration in the stored sample was not observed after visual examination.

3.4. In Vitro Analysis. *3.4.1. In Vitro Release Profile.* In vitro drug release profiles of the PCB-PLGA-CS-NPs and PCB-PLGA-CS-FOL-NPs were performed at both pH 5.5 and

https://doi.org/10.1021/acsabm.4c00853
ACS Appl. Bio Mater. XXXX, XXX, XXX−XXX

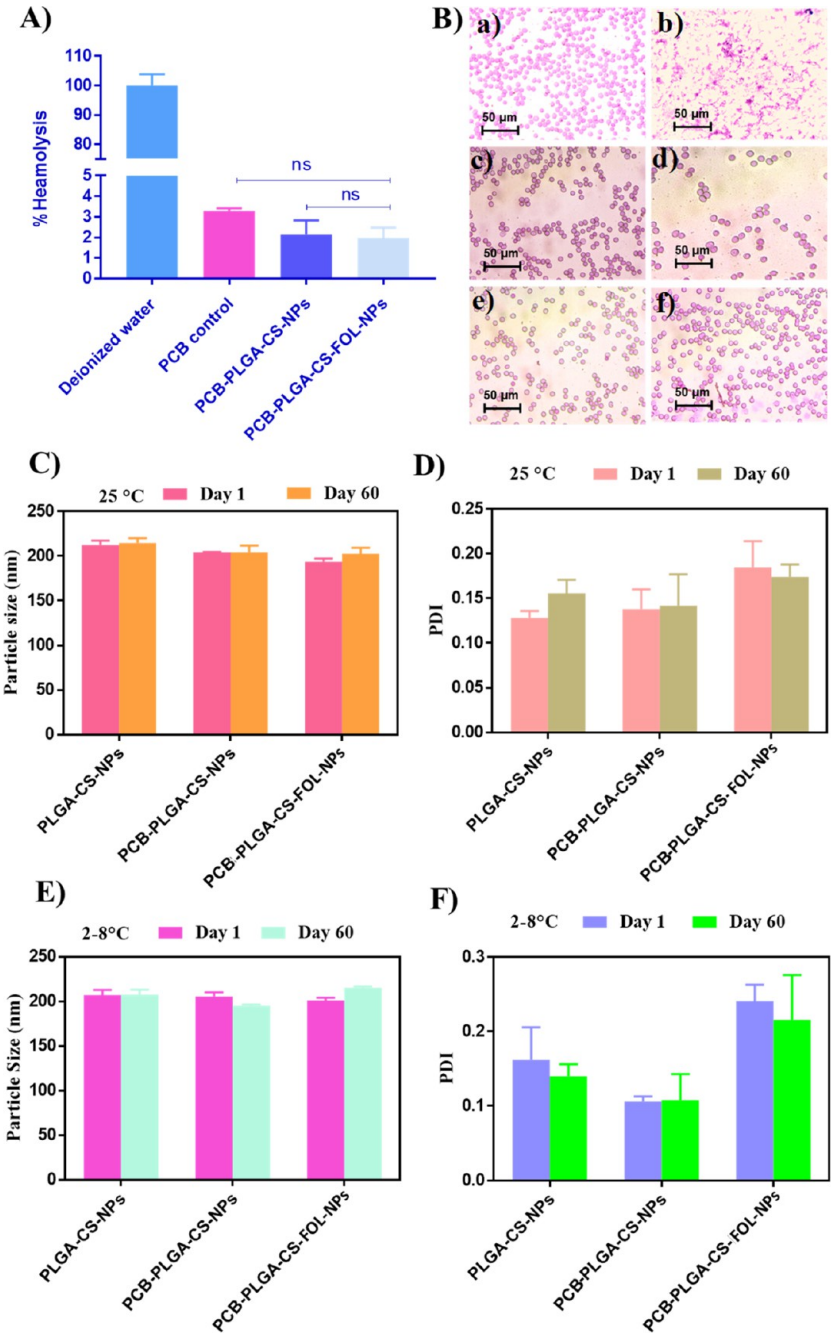

Figure 4. (A) Percentage hemolysis, (B) blood smear images of (a) pure human blood. Human blood treated with (b) distilled water, (c) isotonic saline, (d) PCB suspension, (e) PCB-PLGA-CS-NPs, and (f) PCB-PLGA-CS-FOL-NPs captured at 40× magnification under a bright field microscope. (C) Effect of storage on the particle size of PLGA-CS-NPs, PCB-PLGA-CS-NPs, and PCB-PLGA-CS-FOL-NPs at 25 °C. (D) Effect of storage on PDI of PLGA-CS-NPs, PCB-PLGA-CS-NPs, and PCB-PLGA-CS-FOL-NPs at 25 °C. (E) Effect of storage on the particle size of PLGA-CS-NPs, PCB-PLGA-CS-NPs, and PCB-PLGA-CS-FOL-NPs at 2−8 °C. (F) Effect of storage on PDI of PLGA-CS-NPs, PCB-PLGA-CS-NPs, and PCB-PLGA-CS-FOL-NPs at 2−8 °C.

pH 7.4. (Figure 3B, C). The release study at pH 7.4 revealed 30.81% of PCB-PLGA-CS-NPs and 25.86% of PCB-PLGA-CS-FOL-NPs drug release in the initial 2 h, and by the end of 8 h, 55.2 and 44.3% of drug release were observed. A total of 98.78% of drug release from PCB-PLGA-CS-NPs and 93.54% of drug releases from PCB-PLGA-CS-FOL-NPs were observed at 72 h. The release study at pH 5.5 showed 49.02% of PCB-PLGA-CS-NPs and 60.77% of PCB-PLGA-CS-FOL-NPs drug release in initial 2 h and 68.77%, and by the end of 8 h, 76.33% of the drug was released. At 72 h, 95.40 and 97.06% of drug release was observed. Therefore, PCB-PLGA-CS-FOL-NPs displayed a greater sustained-release profile than PCB-PLGA-CS-NPs, and drug release at pH 5.5 was more rapid than that at pH 7.4. It was done due to significant interaction between drug and polymer, and including a targeting ligand (CS-Folate) in PCB-PLGA-CS-FOL-NPs may have hampered drug release. Furthermore, the PCB release profiles were smooth and continuous in the simulated physiological settings, indicating mixed-order kinetics behavior. T_{50} represents the time taken to release 50% of the loaded drug from nanoformulation. The T_{50}

https://doi.org/10.1021/acsabm.4c00853
ACS Appl. Bio Mater. XXXX, XXX, XXX−XXX

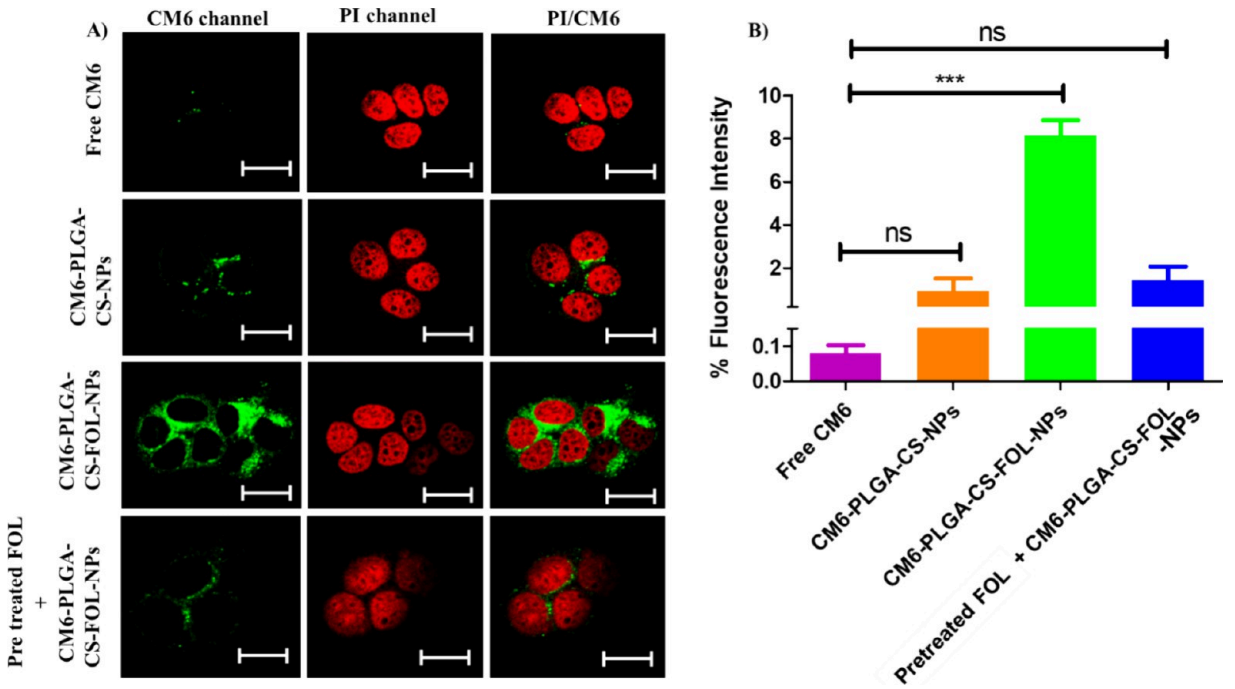

Figure 5. (A) CLSM images revealing the cellular internalization of free CM6, CM6-PLGA-CS-NPs, CM6-PLGA-CS-FOL-NPs, and CM6-PLGA-CS-FOL-NPs pretreated with FOL in MCF-7 cells. The scale bar shows 10 μm. (B) Mean fluorescence intensity of CM6 channels was plotted in a graph showing a significant level of targeted NPs internalization into cells.

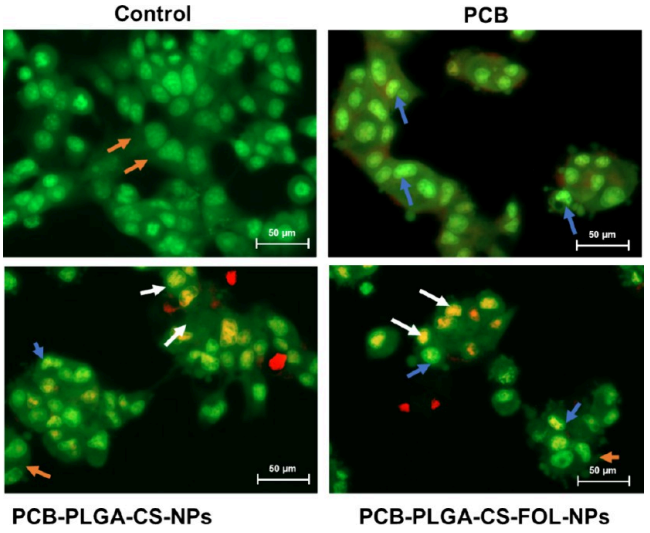

Figure 6. Cellular morphology changes when treated with pure drug (PCB), nontargeted (PCB-PLGA-CS-NPs), and targeted (PCB-PLGA-CS-FOL-NPs) formulation with the IC_{50} of PCB-PLGA-CS-FOL-NPs in MCF-7 cells. MCF-7 cells were observed under fluorescence microscopy using acrylidine orange and ethidium bromide (AO/EtBr) staining. Live cells are designated by the brown arrow, early apoptotic cells by the blue arrow, and late apoptotic cells by the white arrow.

of PCB and different formulations at pH 5.5 and pH 7.4 are presented in Figure 3D. It was observed that T_{50} of the targeted NPs was higher than nontargeted at pH 7.4, which was mainly due to the presence of chitosan-folate in the targeted formulation that has lower solubility at pH 7.4. We have observed that targeted NPs had faster release and lower T_{50} compared to the nontargeted NPs at pH 5.5. This release pattern favors the treatment of cancer due to the acidic microenvironment of cancer cells.[54]

3.4.2. In Vitro Safety Evaluation. 3.4.2.1. Blood Smear. NPs may alter hematological parameters or trigger immunologic responses. As a result, hematological aspects were examined to determine the possible interaction or compatibility of PCB-PLGA-CS-NPs and PCB-PLGA-CS-FOL-NPs using phosphate buffer at pH 7.4 as a negative control and distilled water as a positive control. Following the independent incubation of each sample, a bright field microscope with a 40× magnification was used to examine the blood smear. Light microscopy images of blood smears treated with PCB-PLGA-CS-NPs and PCB-PLGA-CS-FOL-NPs revealed that the size and shape of the blood cells were not significantly altered (Figure 4B).

3.4.2.2. Hemolysis Study. The hemocompatibility of the developed nanoformulations with the blood was evaluated. The % hemolysis induced by the PCB, PCB-PLGA-CS-NPs, and PCB-PLGA-CS-FOL-NPs was found to be 3.214 ± 1.04, 2.474 ± 0.98, and 1.682 ± 0.78%, respectively. The outcomes (Figure 4A) revealed the safety of PCB-PLGA-CS-NPs and PCB-PLGA-CS-FOL-NPs in human blood.

3.4.3. Cellular Uptake Analysis. Multiple studies have demonstrated that the internalization and accumulation of nanomaterials within cells play substantial roles in inducing cell death. To gauge the uptake of CM6-PLGA-CS-FOL-NPs by cancer cells, we incorporated a fluorescent dye named CM6 into these NPs. Then, we measured the intensity of green fluorescence emitted by CM6 within cells to assess the degree of cellular uptake. Confocal microscopy images from the green channel confirmed the presence of internalized CM6-PLGA-CS-FOL-NPs.The pathways through which cells internalize nanoparticles significantly influence the efficacy of drug delivery systems. There are three primary mechanisms involved in the cellular uptake of nanoparticles: endocytosis,

https://doi.org/10.1021/acsabm.4c00853
ACS Appl. Bio Mater. XXXX, XXX, XXX−XXX

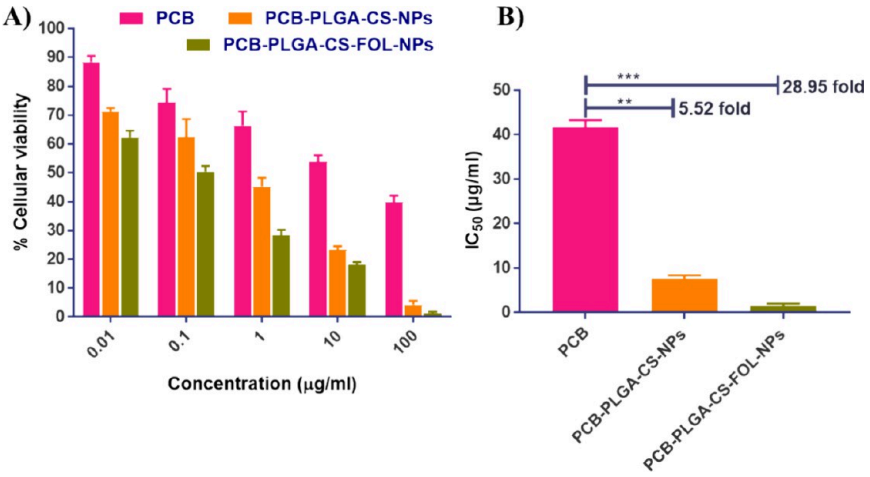

Figure 7. (A) Graphical illustration represents cellular viability of PCB, PCB-PLGA-CS-NPs, and PCB-PLGA-CS-FOL-NPs treated with MCF-7 cells. (B) IC_{50} values were calculated and presented in the graph.

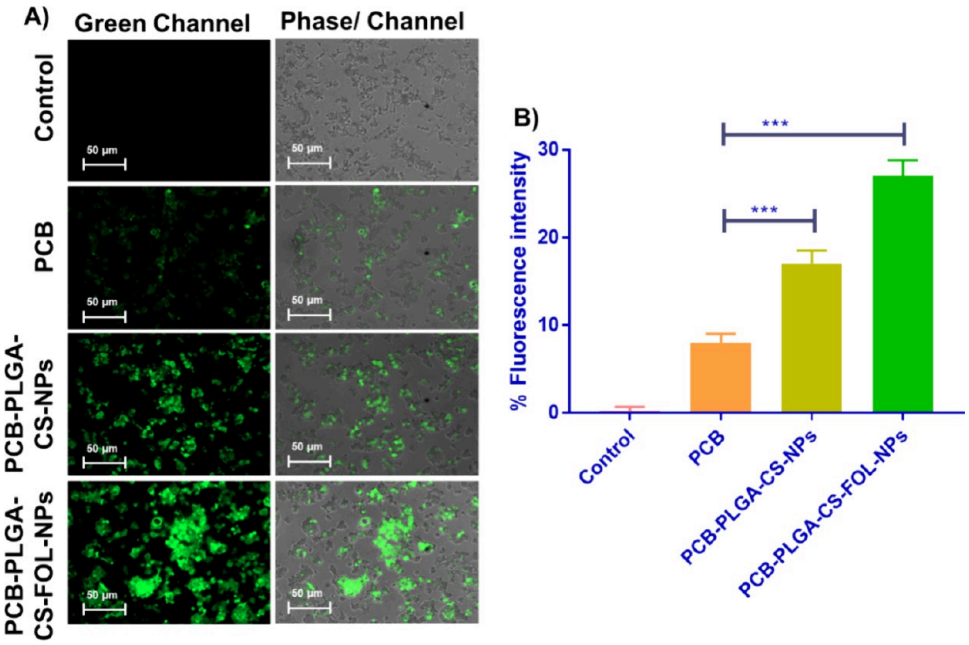

Figure 8. (A) Detection of intracellular ROS generation in MCF-7 cells when incubated with PCB, PCB-PLGA-CS-NPs, and PCB-PLGA-CS-FOL-NPs at the IC_{50} concentration of PCB-PLGA-CS-FOL-NPs. (B) % fluorescent intensity of the green channels.

macropinocytosis (fluid-phase endocytosis), and receptor-mediated endocytosis. Figure 5A shows MCF-7 cells after being incubated with free CM6, CM6-PLGA-CS-FOL-NPs and CM6-PLGA-CS-NPs. The NPs localization in the cell's cytoplasm was more evident in the case of CM6-PLGA-CS-FOL-NPs than in the free CM6 and CM6-PLGA-CS-NPs. According to our investigation, CM6-PLGA-CS-FOL-NPs treated cells have a higher cellular formulation absorption than CM6 alone and CM6-PLGA-CS-NPs treated cells in the MCF-7 cell line (Figure 5B). When MCF-7 cells, which were overexpressed with folate receptors, were pretreated with free folate molecules, these molecules probably occupied the binding sites on the cell surface receptors. This competition notably decreased the receptor-mediated endocytosis of CM6-PLGA-CS-FOL-NPs.

3.4.4. Ao/EtBr Assay (Apoptosis Study). A fluorescence microscopy technique was utilized to observe the morphological features and mechanism of cellular death in MCF-7 produced by PCB, PCB-PLGA-CS-NPs, and PCB-PLGA-CS-FOL-NPs after tagging with AO/EtBr dyes. Figure 6 represents the cellular morphology of the MCF-7 cells following PCB and different formulations. The cytoplasm and nucleus of control MCF-7 (alive and healthy) cells exhibited green fluorescence and normal morphology. Leaving control wells untreated, each well in the plate (PCB, PCB-PLGA-CS-NPs, and PCB-PLGA-CS-FOL-NPs) is treated with the IC_{50} concentration of PCB-PLGA-CS-FOL-NPs. The cells incubated with PCB-PLGA-CS-NPs and PCB-PLGA-CS-FOL-NPs show nuclear morphological modifications, chromatin condensation, and nucleus fragmentation. No such significant changes were observed in the wells of cells treated with PCB. Our results show that PCB-PLGA-CS-NPs and PCB-PLGA-CS-FOL-NPs strongly induce apoptosis in MCF-7 cells compared with PCB drugs.

3.4.5. Cytotoxicity Analysis. An essential technique for evaluating the potential cytotoxic properties of NPs on tumor cells is the assessment of NP-based drug delivery systems using

https://doi.org/10.1021/acsabm.4c00853
ACS Appl. Bio Mater. XXXX, XXX, XXX−XXX

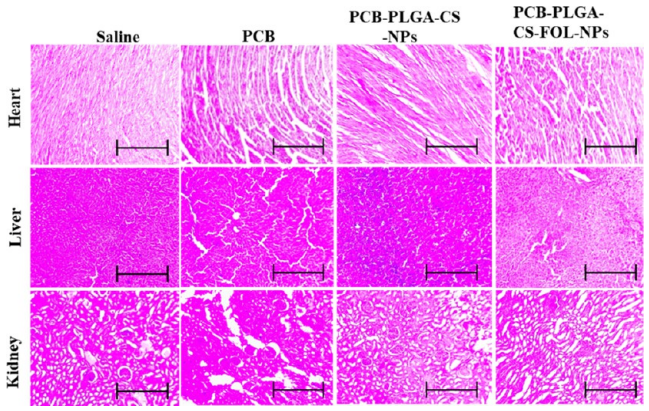

Figure 9. Histological examination of the sections of vital organs such as the heart, liver, and kidney of SD rats after administration of saline, PCB, nontargeted (PCB-PLGA-CS-NPs) and targeted NPs (PCB-PLGA-CS-FOL-NPs). Scale in black showing 100 μm.

cellular viability assays. This assay helps identify the formulations necessary to eliminate 50% of cancer cell populations by assessing their cellular viability. Developing a deeper understanding of NPs' cytotoxicity profiles enables the creation of more effective anticancer therapies. The cytotoxicity assay performed on MCF-7 shows a significant suppression of the proliferation by PCB, PCB-PLGA-CS-NPs, and PCB-PLGA-CS-FOL-NPs. The findings demonstrate that these formulations had a concentration-dependent effect on the viability of the cells (Figure 7A). The IC_{50} of the PCB, PCB-PLGA-CS-NPs, and PCB-PLGA-CS-FOL-NPs for MCF-7 was obtained at 41.6 ± 0.8, 7.55 ± 1.5, and 1.44 ± 1.9 μg/mL (Figure 7B). The results suggest that the formulation of PCB-PLGA-CS-FOL-NPs is more effective compared to PCB and PCB-PLGA-CS-NPs.

3.4.6. Reactive Oxygen Species Analysis. ROS are essentially potent oxidants that have the ability to induce cell death by increasing intracellular reactive radicals that contribute to oxidative damage to lipids, proteins, and DNA. PCB induces a notable increase in ROS levels within the tumor by obstructing the cyclin D3-CDK6 pathway and diminishing the flux of glucose-derived carbon into the pentose phosphate and serine synthesis pathways.[65,66] PCB, PCB-PLGA-CS-NPs, and PCB-PLGA-CS-FOL-NPs effectiveness in the generation of ROS was examined (Figure 8A). In comparison to the control, PCB-PLGA-CS-FOL-NPs possess the higher ability to generate ROS production among the other treated group (PCB and PCB-PLGA-CS-NPs) with an IC_{50} concentration of PCB-PLGA-CS-FOL-NPs that is 1.44 μg/mL (Figure 8B). Therefore, based on the data available, PCB-PLGA-CS-FOL-NPs have more potential for ROS generation than PCB and PCB-PLGA-CS-NPs in MCF-7 cells, which could cause damage to cells and initiate apoptosis.

Intracellular ROS was measured using DCFH-DA. Cells treated with PCB-PLGA-CS-FOL-NPs displayed increased intracellular ROS activity in the MCF-7 cell line compared to the control, cells treated with PCB, and cells treated with PCB-PLGA-CS-NPs.

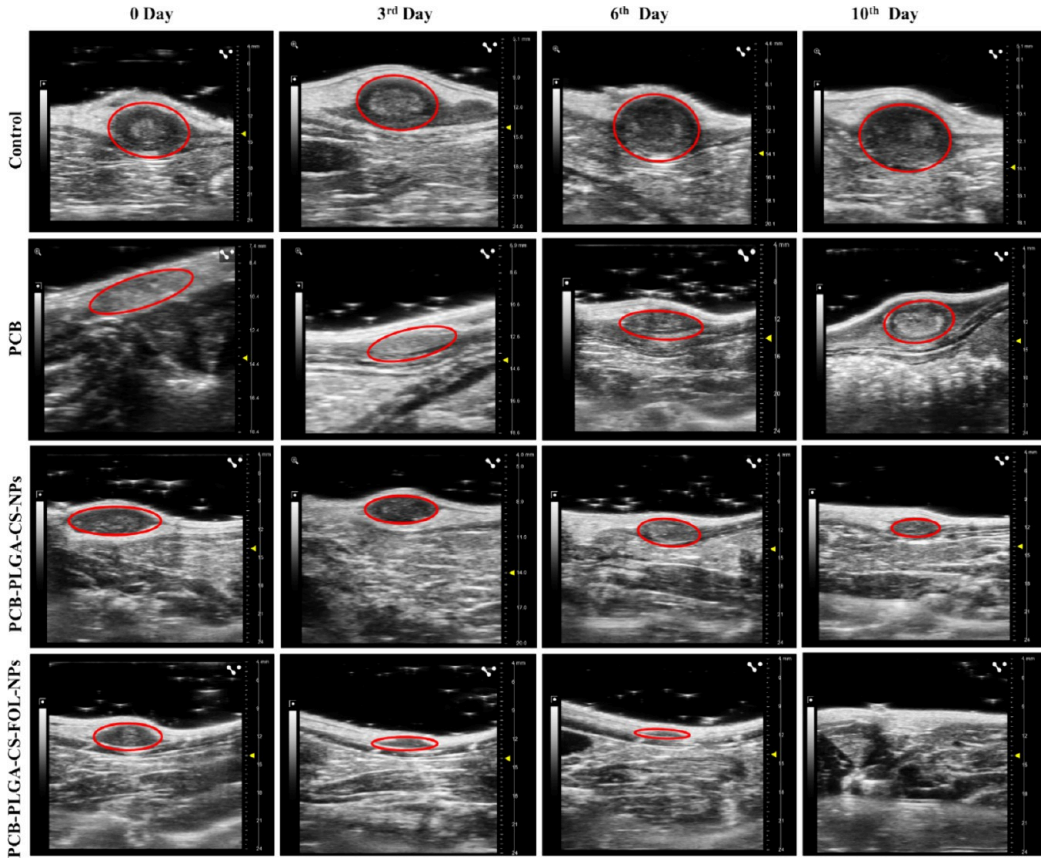

Figure 10. Ultrasound imaging showing breast tumor prior and after administration of PCB, PCB-PLGA-CS-NPs, and PCB-PLGA-CS-FOL-NPs. Images were acquired by using B-mode of the Vivov 3100. Red circle showing tumor location.

https://doi.org/10.1021/acsabm.4c00853
ACS Appl. Bio Mater. XXXX, XXX, XXX−XXX

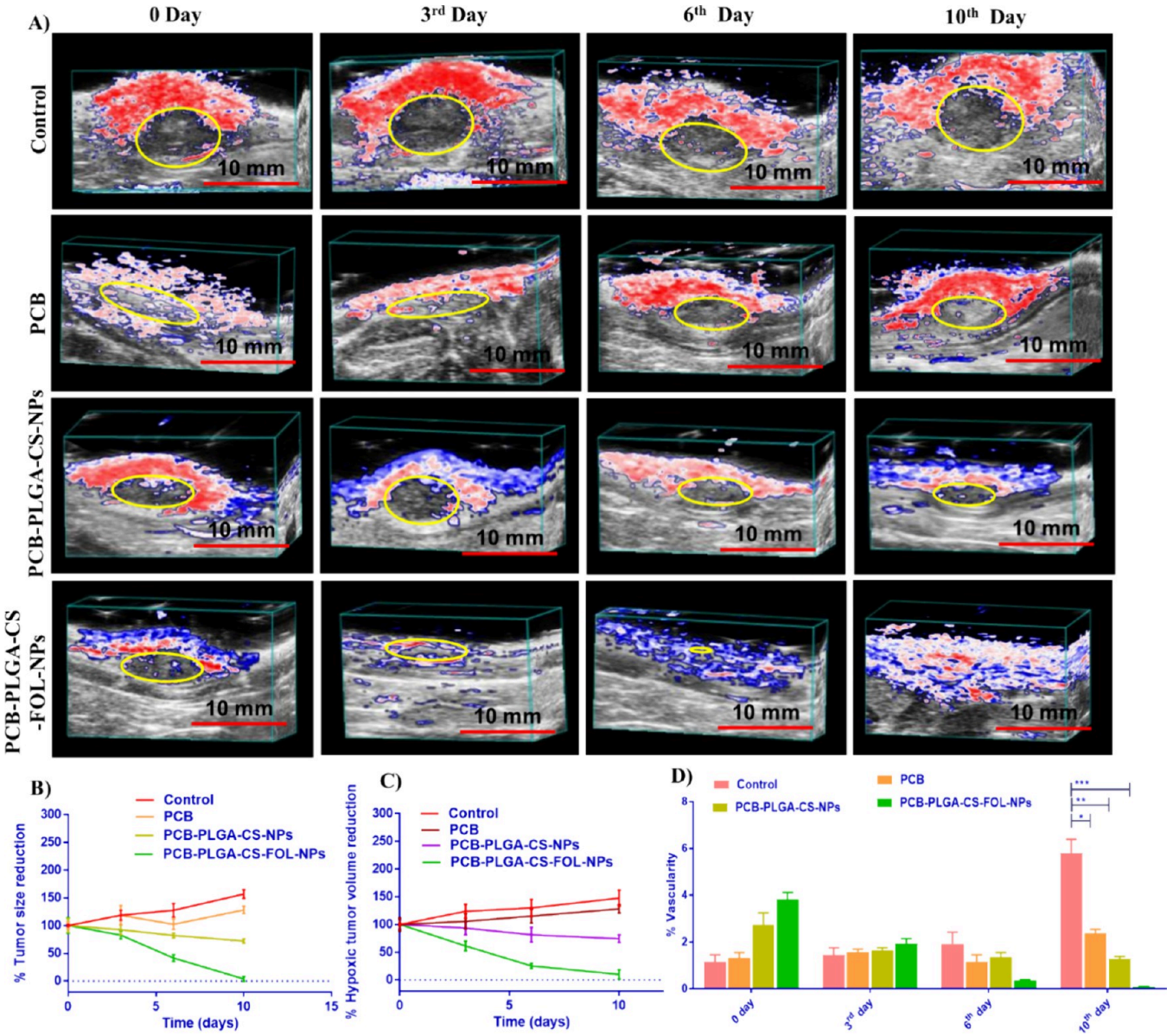

Figure 11. (A) Ultrasound/photoacoustic imaging showing hypoxic tumor volume prior and after administration of PCB, PCB-PLGA-CS-NPs, and PCB-PLGA-CS-FOL-NPs, (B) % tumor volume reduction, (C) % hypoxic tumor volume reduction, and (D) % tumor vascularity of breast tumor. The yellow circle shows the hypoxic tumor region, the red color represents oxygenated blood, and the blue color represents deoxygenated blood.

3.5. In Vivo Analysis. *3.5.1. Histopathological Analysis.* After 15 days of IV injection of the saline, PCB, nontargeted (PCB-PLGA-CS-NPs) and targeted (PCB-PLGA-CS-FOL-NPs) formulations containing the dose of 5.9 mg/kg at the interval of 3 days three times into Sprague−Dawley rats, standard hematoxylin-eosin (H and E) staining was used to assess the morphological properties of the collected heart, liver, and kidney tissues (Figure 9). The control (normal saline solution) treated group in this investigation exhibited no pathological abnormalities in the heart, liver, or kidney. The organs are less damaged in the nontargeted formulation-treated group than those in the PCB control group. Organs such as the heart, liver, and kidney suffer less damage in the targeted formulation-treated group compared to the PCB and nontargeted groups. As a result, the biosafety of PCB-PLGA-CS-NPs and PCB-PLGA-CS-FOL-NPs was demonstrated compared with a commercially available PCB control.

3.5.2. In Vivo Anti-Tumor Activity by Ultrasound and Photoacoustic Imaging. Photoacoustic and ultrasonic imaging was used to analyze rats with chemically induced breast tumors at four different time points: day 0 before the medication and days 3, 6, and 10 after medication. The breast tumor's ultrasound imaging prior to and after PCB, PCB-PLGA-CS-NPs, and PCB-PLGA-CS-FOL-NPs therapy is shown in Figure 10. The research findings indicate a noteworthy decrease in the dimensions of breast tumors after the treatment with targeted NPs. On the other hand, the rats who were not treated and received only saline solution demonstrated a growth in tumor size. However, the group that received only PCB treatment did not exhibit appreciable tumor growth, suggesting that the tumors had stabilized or remained static. In addition, nontargeted PLGA nanoparticles show a small decrease in tumor size (Figure 11B). Hypoxia in tissues happens when cells do not get enough oxygen, which hinders biological functions. Hypoxia is a prevalent characteristic in

https://doi.org/10.1021/acsabm.4c00853
ACS Appl. Bio Mater. XXXX, XXX, XXX−XXX

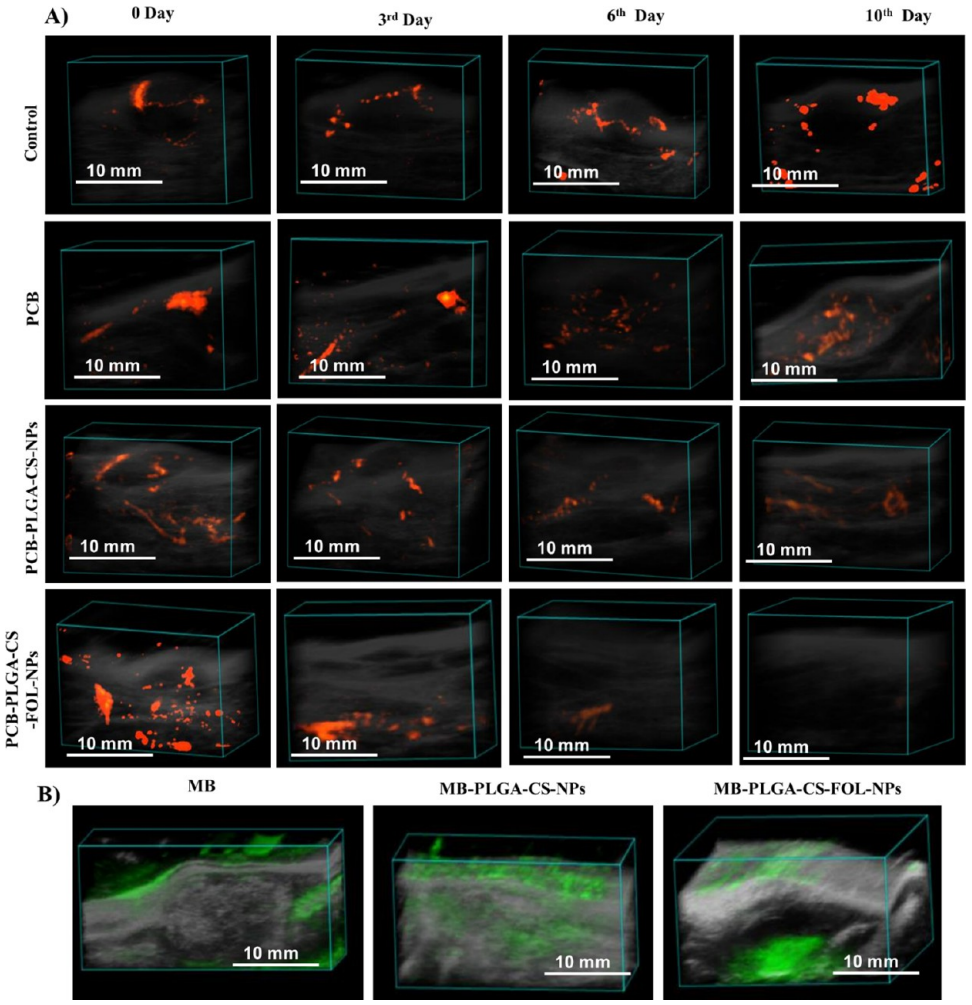

Figure 12. (A) Power Doppler imaging of breast tumor showing tumor vascularity and (B) ultrasound/photoacoustic imaging showing delivery of MB, MB-PLGA-CS-NPs, and MB-PLGA-CS-FOL-NPs to the breast tumor. The red color represents the tumor vascularity and the green color represents the MB distribution.

solid malignant tumors, resulting from insufficient oxygen supply within a range of 70 to 150 μm from the tumor's vascular system. The oxygen deficit is caused by the fast diversification of cancer cells, leading to a situation in which cells are devoid of the essential oxygen required for regular functioning. Hypoxic breast tumors are challenging to treat because their low oxygen content not only affects the tumor cells themselves but also alters the surrounding tissue, creating an environment that is resistant to standard cancer treatments, such as radiation and chemotherapy. Hypoxic tumor volume prior to and after PCB, PCB-PLGA-CS-NPs, and PCB-PLGA-CS-FOL-NPs therapy is depicted in Figure 11A, C. The investigation revealed that targeted NPs could considerably reduce hypoxic tumors compared to nontargeted NPs and pure PCB.

For tumors to continue growing, they need a steady supply of nutrients, which prompts a process called angiogenesis to form new blood vessels both outside and inside the tumor. The administration of PCB-PLGA-CS-FOL-NPs in this experiment yielded a significant outcome. At first, this medication halted the progress of angiogenesis and then showed a steady decrease with time. On the 10th day of therapy, a significant reduction in angiogenesis was detected in the group that received PCB-PLGA-CS-FOL-NPs, as shown in Figure 12A. By the 6th day, the group treated with PCB-PLGA-CS-NPs had a smaller decrease in the tumor vasculature. Nevertheless, on the 10th day, this group demonstrated a noteworthy reduction in tumor angiogenesis. In addition, a group of participants who received only PCB medication in an experimental setting exhibited a modest reduction in the level of tumor angiogenesis. In contrast to these findings, tumor vasculature gradually increased during the 10 days in the control group of rats (Figure 11D). This investigation demonstrates the capacity of PCB-PLGA-CS-FOL-NPs to effectively decrease tumor angiogenesis in comparison to other therapies and the natural growth observed in the control group.

3.5.3. In Vivo Tumor Targeting Efficiency. Photoacoustic pictures of the rat's breast tumors were used to visualize the in vivo distribution of the MB-loaded NPs and MB control after 30 min of intravenous treatment (Figure 12B). The green photoacoustic emissions exposed the existence of the NPs. The breast tumor in the rat model induced with DMBA, treated with MB control, MB-PLGA-CS-NPs, and MB-PLGA-CS-FOL-NPs, exhibited a photoacoustic signal. The research revealed a considerable accumulation of MB-PLGA-CS-FOL-NPs in the breast tumor in comparison to MB-PLGA-CS-NPs and free MB.

https://doi.org/10.1021/acsabm.4c00853
ACS Appl. Bio Mater. XXXX, XXX, XXX−XXX

4. CONCLUSIONS

In this study, we effectively developed and evaluated chitosan folate-targeted PCB-entrapped PLGA nanoparticles for breast cancer imaging and therapy. The solvent evaporation method was used to prepare nontargeted and targeted formulations. Folate receptor-targeted formulation was prepared for improved and targeted therapy of breast cancer. First, we prepared cross-linked chitosan-folate conjugate by using carbodiimide chemistry. CS-FOL conjugation was confirmed by FTIR. The optimized nanoformulations were characterized using DLS, SEM, and TEM for their physicochemical properties, including the particle size, shape, morphology, etc. Z_{avg}, PDI, ZP, and EE of the prepared nanoformulation were found to be in an acceptable range. We also performed XPS, XRD, DSC, and TGA for the surface chemistry and excipient compatibility. In vitro, release investigation confirmed the regulated and long-lasting release of the produced formulation compared to pure PCB.

The hemolytic assay was carried out to check the safety of formulation in human blood, and results showed that prepared nanoformulations were nonhemolytic in human blood. After incubation with the formulations, the blood cell morphology was examined by using a blood smear, and the outcomes revealed that the shape and size of the cells were not substantially changed. We also performed in vitro cellular uptake studies, which showed enhanced uptake of CM6-PLGA-CS-FOL-NPs compared to free CM6 and CM6-PLGA-CS-NPs. Storage stability studies revealed that PCB-PLGA-CS-NPs and PCB-PLGA-CS-FOL-NPs are stable at 25 and 2−8 °C. The IC_{50} values of PCB-PLGA-CS-NPs and PCB-PLGA-CS-FOL-NPs toward the breast cancer cell line were determined to be 7.55 ± 1.5 and 1.44 ± 1.9 μg/mL, respectively. Histopathological examination of sections of vital organs, kidney, heart, and liver of SD rats after treatment with control, drug, nontargeted, and targeted formulation was done. Histopathological images revealed the safety of prepared nanoformulations. Furthermore, in vivo ultrasound and photoacoustic imaging studies demonstrated the targeting efficiencies and therapeutic potential of the developed formulations and were capable of treating hypoxic breast tumors in rat models. In conclusion, PCB-loaded chitosan folate-targeted PLGA nanoparticles can be potential candidates for breast cancer imaging and therapy.

■ ASSOCIATED CONTENT

Supporting Information

The Supporting Information is available free of charge at https://pubs.acs.org/doi/10.1021/acsabm.4c00853.

FTIR spectra of CS, FOL, and CS-FOL; FTIR peak assignment of CS, FOL, and CS-FOL (PDF)

■ AUTHOR INFORMATION

Corresponding Authors

Biplob Koch − *Genotoxicology and Cancer Biology Lab, Department of Zoology, Institute of Science, Banaras Hindu University, Varanasi 221005 U.P., India;* orcid.org/0000-0001-9093-7793; Email: biplob@bhu.ac.in

Madaswamy S. Muthu − *Department of Pharmaceutical Engineering and Technology, Indian Institute of Technology (BHU), Varanasi 221005 U.P., India;* orcid.org/0000-0001-5805-7921; Phone: +91 9235195928; Email: msmuthu.phe@itbhu.ac.in; Fax: +91 542 2368428

Authors

Abhishesh Kumar Mehata − *Department of Pharmaceutical Engineering and Technology, Indian Institute of Technology (BHU), Varanasi 221005 U.P., India*

Jyoti Bonlawar − *Department of Pharmaceutical Engineering and Technology, Indian Institute of Technology (BHU), Varanasi 221005 U.P., India*

Rupen Tamang − *Genotoxicology and Cancer Biology Lab, Department of Zoology, Institute of Science, Banaras Hindu University, Varanasi 221005 U.P., India*

Ankit Kumar Malik − *Department of Pharmaceutical Engineering and Technology, Indian Institute of Technology (BHU), Varanasi 221005 U.P., India*

Aseem Setia − *Department of Pharmaceutical Engineering and Technology, Indian Institute of Technology (BHU), Varanasi 221005 U.P., India*

Shailendra Kumar − *SATHI, Central Discovery Centre, Banaras Hindu University, Varanasi 221005 U.P., India*

Ranadheer Reddy Challa − *Department of Pharmaceutical Science, School of Applied Sciences and Humanities, VIGNAN's Foundation for Science, Technology & Research, Vadlamudi 522213 Andhra Pradesh, India*

Bhaskar Vallamkonda − *Department of Pharmaceutical Science, School of Applied Sciences and Humanities, VIGNAN's Foundation for Science, Technology & Research, Vadlamudi 522213 Andhra Pradesh, India*

Complete contact information is available at: https://pubs.acs.org/10.1021/acsabm.4c00853

Author Contributions

⊥A.K.M. and J.B. contributed equally.

Notes

The authors declare no competing financial interest.

■ ACKNOWLEDGMENTS

The authors gratefully acknowledge the financial support from MHRD and IIT BHU, Varanasi, India, and CDC-SATHI BHU for imaging studies. The author B.K. acknowledges Banaras Hindu University for providing funds under the IoE scheme (File No.R/Dev/D/IoE/Incentive/2021-22/32449.

■ REFERENCES

(1) DeSantis, C.; Siegel, R.; Jemal, A.*Breast Cancer Facts & Figures 2015−2016*. Am. Cancer Soc.: 2015; Vol. *44*, pp 1−44.

(2) Flaherty, D. C.; Bawa, R.; Burton, C.; Goldfarb, M. Breast Cancer in Male Adolescents and Young Adults. *Ann. Surg Oncol* **2017**, *24* (1), 84−90.

(3) Sung, H.; Ferlay, J.; Siegel, R. L.; Laversanne, M.; Soerjomataram, I.; Jemal, A.; Bray, F. Global Cancer Statistics 2020: Globocan Estimates of Incidence and Mortality Worldwide for 36 Cancers in 185 Countries. *CA Cancer J. Clin* **2021**, *71* (3), 209−249.

(4) Stevenson, J.; Farmer, R. Hrt and Breast Cancer: A Million Women Ride Again. *Climacteric* **2020**, *23* (3), 226−228.

(5) Weigelt, B.; Reis-Filho, J. S. Histological and Molecular Types of Breast Cancer: Is There a Unifying Taxonomy? *Nat. Rev. Clin. Oncol.* **2009**, *6* (12), 718−730.

(6) Jordan, R. M.; Oxenberg, J. Breast Cancer Conservation Therapy. In *Statpearls*; StatPearls Publishing Copyright © 2023, StatPearls Publishing LLC: Treasure Island (FL), 2023.

(7) Bonlawar, J.; Setia, A.; Challa, R. R.; Vallamkonda, B.; Mehata, A. K.; Vaishali; Viswanadh, M. K.; Muthu, M. S. Targeted Nanotheransotics: Integration of Preclinical Mri and Ct in the

Molecular Imaging and Therapy of Advanced Diseases. *Nanotheranostics* **2024**, *8* (3), 401−426.
(8) Yao, Y.; Zhou, Y.; Liu, L.; Xu, Y.; Chen, Q.; Wang, Y.; Wu, S.; Deng, Y.; Zhang, J.; Shao, A. Nanoparticle-Based Drug Delivery in Cancer Therapy and Its Role in Overcoming Drug Resistance. *Front. Mol. Biosci.* **2020**, *7*, 193.
(9) Tagde, P.; Najda, A.; Nagpal, K.; Kulkarni, G. T.; Shah, M.; Ullah, O.; Balant, S.; Rahman, M. H. Nanomedicine-Based Delivery Strategies for Breast Cancer Treatment and Management. *Int. J. Mol. Sci.* **2022**, *23* (5), 2856.
(10) Shen, S.; Clairambault, J. Cell Plasticity in Cancer Cell Populations. *F1000Research* **2020**, *9*, 365.
(11) Tabatabaei Mirakabad, F. S.; Nejati-Koshki, K.; Akbarzadeh, A.; Yamchi, M. R.; Milani, M.; Zarghami, N.; Zeighamian, V.; Rahimzadeh, A.; Alimohammadi, S.; Hanifehpour, Y.; et al. PLGA-Based Nanoparticles as Cancer Drug Delivery Systems. *Asian Pac. J. Cancer Prev.* **2014**, *15* (2), 517−535.
(12) Wang, Y.; Li, P.; Truong-Dinh Tran, T.; Zhang, J.; Kong, L. Manufacturing Techniques and Surface Engineering of Polymer Based Nanoparticles for Targeted Drug Delivery to Cancer. *Nanomaterials* **2016**, *6* (2), 26.
(13) Khalili, L.; Dehghan, G.; Sheibani, N.; Khataee, A. Smart Active-Targeting of Lipid-Polymer Hybrid Nanoparticles for Therapeutic Applications: Recent Advances and Challenges. *Int. J. Biol. Macromol.* **2022**, *213*, 166−194.
(14) Setia, A.; Vallamkonda, B.; Challa, R. R.; Mehata, A. K.; Badgujar, P.; Muthu, M. S. Herbal Theranostics: Controlled, Targeted Delivery and Imaging of Herbal Molecules. *Nanotheranostics* **2024**, *8* (3), 344−379.
(15) Kim, E. S.; Scott, L. J. Palbociclib: A Review in Hr-Positive, Her2-Negative, Advanced or Metastatic Breast Cancer. *Target Oncol* **2017**, *12* (3), 373−383.
(16) Rocca, A.; Farolfi, A.; Bravaccini, S.; Schirone, A.; Amadori, D. Palbociclib (Pd 0332991): Targeting the Cell Cycle Machinery in Breast Cancer. *Expert Opin Pharmacother* **2014**, *15* (3), 407−420.
(17) Makadia, H. K.; Siegel, S. J. Poly Lactic-Co-Glycolic Acid (Plga) as Biodegradable Controlled Drug Delivery Carrier. *Polymers (Basel)* **2011**, *3* (3), 1377−1397.
(18) Hines, D. J.; Kaplan, D. L. Poly(Lactic-Co-Glycolic) Acid-Controlled-Release Systems: Experimental and Modeling Insights. *Crit Rev. Ther Drug Carrier Syst* **2013**, *30* (3), 257−276.
(19) Athira, T.; Selvaraju, K.; Gowrishankar, N. Biodegradable Polymeric Nanoparticles: The Novel Carrier for Controlled Release Drug Delivery System. *Int. J. Sci. Res. Arch.* **2023**, *8* (1), 630−637.
(20) Zolnik, B. S.; Burgess, D. J. Evaluation of in Vivo-in Vitro Release of Dexamethasone from Plga Microspheres. *J. Controlled Release* **2008**, *127* (2), 137−145.
(21) Fini, A.; Orienti, I. The Role of Chitosan in Drug Delivery: Current and Potential Applications. *Am. J. Adv. Drug Delivery* **2003**, *1*, 43−59.
(22) Talaei, A.; Ashori, A.; Heydari, V. A Comparative Study on the Mechanical and Physical Properties of Plywood Panels Prepared by Chitosan as Bio-Adhesive. *J. Environ. Polym. Degrad.* **2022**, *30* (10), 4263−4270.
(23) Alhodieb, F. S.; Barkat, M. A.; Barkat, H. A.; Ab Hadi, H.; Khan, M. I.; Ashfaq, F.; Rahman, M. A.; Hassan, M. Z.; et al. Chitosan-Modified Nanocarriers as Carriers for Anticancer Drug Delivery: Promises and Hurdles. *Int. J. Biol. Macromol.* **2022**, *217*, 457−469.
(24) Palao-Suay, R.; Aguilar, M. R.; Parra-Ruiz, F. J.; Fernández-Gutiérrez, M.; Parra, J.; Sánchez-Rodríguez, C.; Sanz-Fernández, R.; Rodrigáñez, L.; Román, J. S. Anticancer and Antiangiogenic Activity of Surfactant-Free Nanoparticles Based on Self-Assembled Polymeric Derivatives of Vitamin E: Structure-Activity Relationship. *Biomacromolecules* **2015**, *16* (5), 1566−1581.
(25) Mehata, A. K.; Setia, A.; Malik, A. K.; Hassani, R.; Dailah, H. G.; Alhazmi, H. A.; Albarraq, A. A.; Mohan, S.; Muthu, M. S. Vitamin E Tpgs-Based Nanomedicine, Nanotheranostics, and Targeted Drug Delivery: Past, Present, and Future. *Pharmaceutics* **2023**, *15* (3), 722.
(26) Ha, E. S.; Baek, I. h.; Kim, M. S. Preparation and Characterization of Tpgs-Colloidal Silica Microparticles for Enhancement of Solubility and Oral Bioavailability of Lercanidipine Hydrochloride. *Bull. Korean Chem. Soc.* **2016**, *37* (5), 660−666.
(27) Husain, A.; Makadia, V.; Valicherla, G. R.; Riyazuddin, M.; Gayen, J. R. Approaches to Minimize the Effects of P-Glycoprotein in Drug Transport: A Review. *Drug Dev. Res.* **2022**, *83* (4), 825−841.
(28) Tuguntaev, R. G.; Chen, S.; Eltahan, A. S.; Mozhi, A.; Jin, S.; Zhang, J.; Li, C.; Wang, P. C.; Liang, X. J. P-Gp Inhibition and Mitochondrial Impairment by Dual-Functional Nanostructure Based on Vitamin E Derivatives to Overcome Multidrug Resistance. *ACS Appl. Mater. Interfaces* **2017**, *9* (20), 16900−16912.
(29) Birringer, M.; Pfluger, P.; Kluth, D.; Landes, N.; Brigelius-Flohé, R. Identities and Differences in the Metabolism of Tocotrienols and Tocopherols in Hepg2 Cells. *J. Nutr.* **2002**, *132* (10), 3113−3118.
(30) Chow, L. W.; Cheung, M. N.; Loo, W. T.; Guan, X. Y. A Rat Cell Line Derived from Dmba-Induced Mammary Carcinoma. *Life Sci.* **2003**, *73* (1), 27−40.
(31) Ramadhani, A. H.; Ahkam, A. H.; Suharto, A. R.; Jatmiko, Y. D.; Tsuboi, H.; Rifa'i, M. Suppression of Hypoxia and Inflammatory Pathways by Phyllanthus Niruri Extract Inhibits Angiogenesis in Dmba-Induced Breast Cancer Mice. *Res. Pharm. Sci.* **2021**, *16* (2), 217−226.
(32) O'Shannessy, D. J.; Somers, E. B.; Maltzman, J.; Smale, R.; Fu, Y. S. Folate Receptor Alpha (Fra) Expression in Breast Cancer: Identification of a New Molecular Subtype and Association with Triple Negative Disease. *Springerplus* **2012**, *1*, 22.
(33) Lucock, M. Folic Acid: Nutritional Biochemistry, Molecular Biology, and Role in Disease Processes. *Mol. Genet. Metab.* **2000**, *71* (1−2), 121−138.
(34) Jeon, M.; Song, W.; Huynh, E.; Kim, J.; Kim, J.; Helfield, B. L.; Leung, B. Y.; Goertz, D. E.; Zheng, G.; Oh, J.; Lovell, J. F.; Kim, C. Methylene Blue Microbubbles as a Model Dual-Modality Contrast Agent for Ultrasound and Activatable Photoacoustic Imaging. *J. Biomed. Opt.* **2014**, *19* (1), 16005.
(35) Chen, Z.; Chattaraj, R.; Pulsipher, K. W.; Karmacharya, M. B.; Hammer, D. A.; Lee, D.; Sehgal, C. M. Photoacoustic and Ultrasound Dual-Mode Imaging Via Functionalization of Recombinant Protein-Stabilized Microbubbles with Methylene Blue. *ACS Appl. Bio Mater.* **2019**, *2* (9), 4020−4026.
(36) Rajana, N.; Sandeep Chary, P.; Bhavana, V.; Deshmukh, R.; Dukka, K.; Sharma, A.; Kumar Mehra, N. Targeted Delivery and Apoptosis Induction of CDK-4/6 Inhibitor Loaded Folic Acid Decorated Lipid-Polymer Hybrid Nanoparticles in Breast Cancer Cells. *Int. J. Pharm.* **2024**, *651*, No. 123787.
(37) Dhamija, P.; Mehata, A. K.; Tamang, R.; Bonlawar, J.; Vaishali; Malik, A. K.; Setia, A.; Kumar, S.; Challa, R. R.; Koch, B.; Muthu, M. S. Redox-Sensitive Poly(Lactic-Co-Glycolic Acid) Nanoparticles of Palbociclib: Development, Ultrasound/Photoacoustic Imaging, and Smart Breast Cancer Therapy. *Mol. Pharmaceutics* **2024**, *21* (6), 2713−2726.
(38) Mansouri, S.; Cuie, Y.; Winnik, F.; Shi, Q.; Lavigne, P.; Benderdour, M.; Beaumont, E.; Fernandes, J. C. Characterization of Folate-Chitosan-DNA Nanoparticles for Gene Therapy. *Biomaterials* **2006**, *27* (9), 2060−2065.
(39) Li, Y.; Zou, Z.; An, J.; Liu, X.; Wu, Q.; Sun, J.; Liu, X.; Du, J.; Xiong, Y.; Wu, C.; Mei, X.; Tian, H. Folic Acid-Functionalized Chitosan Nanoparticles with Bioenzyme Activity for the Treatment of Spinal Cord Injury. *Eur. J. Pharm. Sci.* **2024**, *192*, No. 106667.
(40) Stella, B.; Arpicco, S.; Peracchia, M. T.; Desmaële, D.; Hoebeke, J.; Renoir, M.; D'Angelo, J.; Cattel, L.; Couvreur, P. Design of Folic Acid-Conjugated Nanoparticles for Drug Targeting. *J. Pharm. Sci.* **2000**, *89* (11), 1452−1464.
(41) Esfandiarpour-Boroujeni, S.; Bagheri-Khoulenjani, S.; Mirzadeh, H.; Amanpour, S. Fabrication and Study of Curcumin Loaded Nanoparticles Based on Folate-Chitosan for Breast Cancer Therapy Application. *Carbohydr. Polym.* **2017**, *168*, 14−21.

https://doi.org/10.1021/acsabm.4c00853
ACS Appl. Bio Mater. XXXX, XXX, XXX−XXX

(42) Kızılbey, K. Optimization of Rutin-Loaded Plga Nanoparticles Synthesized by Single-Emulsion Solvent Evaporation Method. *Acs Omega* **2019**, *4* (1), 555−562.
(43) Derman, S. Caffeic Acid Phenethyl Ester Loaded Plga Nanoparticles: Effect of Various Process Parameters on Reaction Yield, Encapsulation Efficiency, and Particle Size. *J. Nanomater.* **2016**, *16* (1), 318.
(44) Havrdova, M.; Polakova, K.; Skopalik, J.; Vujtek, M.; Mokdad, A.; Homolkova, M.; Tucek, J.; Nebesarova, J.; Zboril, R. Field Emission Scanning Electron Microscopy (Fe-Sem) as an Approach for Nanoparticle Detection inside Cells. *Micron* **2014**, *67*, 149−154.
(45) Tizro, P.; Choi, C.; Khanlou, N. Sample Preparation for Transmission Electron Microscopy. *Methods Mol. Biol.* **2019**, *1897*, 417−424.
(46) Varshosaz, J.; Hassanzadeh, F.; Sadeghi Aliabadi, H.; Nayebsadrian, M.; Banitalebi, M.; Rostami, M. Synthesis and Characterization of Folate-Targeted Dextran/Retinoic Acid Micelles for Doxorubicin Delivery in Acute Leukemia. *BioMed Res. Int.* **2014**, *2014*, No. 525684.
(47) Lippi, G.; Franchini, M.; Targher, G. Arterial Thrombus Formation in Cardiovascular Disease. *Nature Reviews Cardiology* **2011**, *8* (9), 502−512.
(48) Gill, P.; Moghadam, T. T.; Ranjbar, B. Differential Scanning Calorimetry Techniques: Applications in Biology and Nanoscience. *J. Biomol. Tech.* **2010**, *21* (4), 167−193.
(49) Xiong, S.; George, S.; Ji, Z.; Lin, S.; Yu, H.; Damoiseaux, R.; France, B.; Ng, K. W.; Loo, S. C. Size of Tio(2) Nanoparticles Influences Their Phototoxicity: An in Vitro Investigation. *Arch. Toxicol.* **2013**, *87* (1), 99−109.
(50) de Britto, D.; de Moura, M. R.; Aouada, F. A.; Pinola, F. G.; Lundstedt, L. M.; Assis, O. B.; Mattoso, L. H. Entrapment Characteristics of Hydrosoluble Vitamins Loaded into Chitosan and N, N, N-Trimethyl Chitosan Nanoparticles. *Macromol. Res.* **2014**, *22*, 1261−1267.
(51) Farmoudeh, A.; Saeedi, M.; Talavaki, F.; Ghasemi, M.; Akbari, J.; Nokhodchi, A. Methylene Blue Loaded Solid Lipid Nanoparticles: Preparation, Optimization, and in-Vivo Burn Healing Assessment. *J. Drug Delivery Sci. Technol.* **2022**, *70*, No. 103209.
(52) Vikas; Viswanadh, M. K.; Mehata, A. K.; Sharma, V.; Priya, V.; Varshney, N.; Mahto, S. K.; Muthu, M. S. Bioadhesive Chitosan Nanoparticles: Dual Targeting and Pharmacokinetic Aspects for Advanced Lung Cancer Treatment. *Carbohydr. Polym.* **2021**, *274*, No. 118617.
(53) Kim, B.; Hosn, R. R.; Remba, T.; Yun, D.; Li, N.; Abraham, W.; Melo, M. B.; Cortes, M.; Li, B.; Zhang, Y.; Dong, Y.; Irvine, D. J. Optimization of Storage Conditions for Lipid Nanoparticle-Formulated Self-Replicating Rna Vaccines. *J. Controlled Release* **2023**, *353*, 241−253.
(54) Ak, G.; Yilmaz, H.; Güneş, A.; Hamarat Sanlier, S. In Vitro and in Vivo Evaluation of Folate Receptor-Targeted a Novel Magnetic Drug Delivery System for Ovarian Cancer Therapy. *Artif Cells Nanomed Biotechnol* **2018**, *46* (sup1), 926−937.
(55) de la Harpe, K. M.; Kondiah, P. P. D.; Choonara, Y. E.; Marimuthu, T.; du Toit, L. C.; Pillay, V. The Hemocompatibility of Nanoparticles: A Review of Cell-Nanoparticle Interactions and Hemostasis. *Cells* **2019**, *8* (10), 1209.
(56) Neun, B. W.; Ilinskaya, A. N.; Dobrovolskaia, M. A. Updated Method for in Vitro Analysis of Nanoparticle Hemolytic Properties. *Methods Mol. Biol.* **2018**, *1682*, 91−102.
(57) Dubey, R. D.; Alam, N.; Saneja, A.; Khare, V.; Kumar, A.; Vaidh, S.; Mahajan, G.; Sharma, P. R.; Singh, S. K.; Mondhe, D. M.; Gupta, P. N. Development and Evaluation of Folate Functionalized Albumin Nanoparticles for Targeted Delivery of Gemcitabine. *Int. J. Pharm.* **2015**, *492* (1−2), 80−91.
(58) Barzegar, E.; Fouladdel, S.; Movahhed, T. K.; Atashpour, S.; Ghahremani, M. H.; Ostad, S. N.; Azizi, E. Effects of Berberine on Proliferation, Cell Cycle Distribution and Apoptosis of Human Breast Cancer T47d and Mcf7 Cell Lines. *Iran. J. Basic Med. Sci.* **2015**, *18* (4), 334−342.
(59) Cai, L.; Yu, R.; Hao, X.; Ding, X. Folate Receptor-Targeted Bioflavonoid Genistein-Loaded Chitosan Nanoparticles for Enhanced Anticancer Effect in Cervical Cancers. *Nanoscale Res. Lett.* **2017**, *12* (1), 509.
(60) Singh, R. P.; Sharma, G.; Sonali; Singh, S.; Kumar, M.; Pandey, B. L.; Koch, B.; Muthu, M. S. Vitamin E Tpgs Conjugated Carbon Nanotubes Improved Efficacy of Docetaxel with Safety for Lung Cancer Treatment. *Colloids Surf. B Biointerfaces* **2016**, *141*, 429−442.
(61) Shen, J. M.; Gao, F. Y.; Yin, T.; Zhang, H. X.; Ma, M.; Yang, Y. J.; Yue, F. Crgd-Functionalized Polymeric Magnetic Nanoparticles as a Dual-Drug Delivery System for Safe Targeted Cancer Therapy. *Pharmacol. Res.* **2013**, *70* (1), 102−115.
(62) Dudhipala, N.; Puchchakayala, G. Capecitabine Lipid Nanoparticles for Anti-Colon Cancer Activity in 1,2-Dimethylhydrazine-Induced Colon Cancer: Preparation, Cytotoxic, Pharmacokinetic, and Pathological Evaluation. *Drug Dev. Ind. Pharm.* **2018**, *44* (10), 1572−1582.
(63) Raes, F.; Sobilo, J.; Le Mée, M.; Rétif, S.; Natkunarajah, S.; Lerondel, S.; Le Pape, A. High Resolution Ultrasound and Photoacoustic Imaging of Orthotopic Lung Cancer in Mice: New Perspectives for Onco-Pharmacology. *PLoS One* **2016**, *11* (4), No. e0153532.
(64) Wang, H.; Liu, C.; Gong, X.; Hu, D.; Lin, R.; Sheng, Z.; Zheng, C.; Yan, M.; Chen, J.; Cai, L.; Song, L. In Vivo Photoacoustic Molecular Imaging of Breast Carcinoma with Folate Receptor-Targeted Indocyanine Green Nanoprobes. *Nanoscale* **2014**, *6* (23), 14270−14279.
(65) Stefanatos, R.; Sanz, A. The Role of Mitochondrial Ros in the Aging Brain. *FEBS Lett.* **2018**, *592* (5), 743−758.
(66) Chen, Y.; Luo, X.; Zou, Z.; Liang, Y. The Role of Reactive Oxygen Species in Tumor Treatment and Its Impact on Bone Marrow Hematopoiesis. *Curr. Drug Targets* **2020**, *21* (5), 477−498.

https://doi.org/10.1021/acsabm.4c00853
ACS Appl. Bio Mater. XXXX, XXX, XXX−XXX